561817
P42

NASA TN D-1926

41p

TECHNICAL NOTE

D-1926

TRANSONIC INVESTIGATION OF THE EFFECTS OF

NOSE BLUNTNESS, FINENESS RATIO, CONE ANGLE, AND BASE SHAPE

ON THE STATIC AERODYNAMIC CHARACTERISTICS OF SHORT,

BLUNT CONES AT ANGLES OF ATTACK TO 180°

By Cuyler W. Brooks, Jr., and Charles D. Trescot, Jr.

Langley Research Center
Langley Station, Hampton, Va.   602/448

NATIONAL AERONAUTICS AND SPACE ADMINISTRATION

WASHINGTON   August 1963

NATIONAL AERONAUTICS AND SPACE ADMINISTRATION

TECHNICAL NOTE D-1926

TRANSONIC INVESTIGATION OF THE EFFECTS OF

NOSE BLUNTNESS, FINENESS RATIO, CONE ANGLE, AND BASE SHAPE

ON THE STATIC AERODYNAMIC CHARACTERISTICS OF SHORT,

BLUNT CONES AT ANGLES OF ATTACK TO 180°

By Cuyler W. Brooks, Jr., and Charles D. Trescot, Jr.

SUMMARY

/8 889

An investigation has been conducted in the Langley transonic blowdown tunnel to determine the effects of variations in Mach number, nose bluntness, fineness ratio, cone semiangle, and base shape on the static longitudinal characteristics of low-fineness-ratio blunted cones. The tests were made at Mach numbers from about 0.8 to 1.2 through an angle-of-attack range that generally varied from 0° to 180°. Reynolds number, based upon the base diameter, varied from 3.67×10^6 to 5.32×10^6.

The results of the investigation indicate that all shapes tested have a stable trim point at an angle of attack of 180° that is undesirable for a passive entry body designed to enter along a purely ballistic path. Variations in Mach number, nose bluntness, cone semiangle, and base shape had no significant effect on the static stability, but increases in fineness ratio caused decreases in stability at angles of attack up to 45° with the moment reference center located at two-thirds of the body length from the nose. Increases in fineness ratio and decreases in cone semiangle generally caused an increase in normal force over most of the test angle-of-attack range. Variations in nose bluntness and base shape had little or no effect on normal-force coefficient. At angles of attack up to about 160°, increases in fineness ratio generally caused a reduction in the absolute values of axial force. In general, variations in cone semiangle had little effect on axial force, except at angles of attack near 0° at Mach numbers of 0.8 and 1.2 and near 90° at M = 0.8. Variations in nose bluntness and base shape below 80° angle of attack had little or no effect on axial force, but at angles of attack from 80° to 180°, varying the base shape from convex to concave caused, in general, a large increase in the absolute values of axial force.

INTRODUCTION

The National Aeronautics and Space Administration is conducting an investigation to obtain systematic information from low subsonic to hypersonic speeds on

bodies of a type that can be used for unmanned, passive, planetary probes. The selection of a shape for this type of probe must take into account the effects of the geometric parameters that influence not only the heating problems but also the static and dynamic stability. For blunt, low-fineness-ratio cones (a type considered for a Venus or Mars passive probe), the important geometric parameters include nose bluntness, base shape, cone semiangle, and body fineness ratio. The stability of the vehicle should be such that the vehicle will assume and remain in a nose-forward attitude ($\alpha = 0^{\circ}$) during the entire entry phase even though initial entry may be made at angles of attack up to 180°.

This paper presents the results of a transonic investigation of low-fineness-ratio blunted cones intended for use primarily as unmanned planetary probes. The results show the effect of variations in nose bluntness, cone semiangle, base shape, and fineness ratio on the static longitudinal aerodynamic characteristics. The tests were made in the 26-inch Langley transonic blowdown tunnel at Mach numbers from about 0.8 to 1.2 through an angle-of-attack range that generally varied from 0° to 180°. Reference 1 presents the results of tests at supersonic speeds at angles of attack to 180° on bodies essentially identical to those of the present tests. Results showing the effects of variations in some of the geometric parameters mentioned on the longitudinal aerodynamic characteristics of other blunt ballistic bodies over various low angle-of-attack ranges at transonic speeds are presented in references 2 through 5.

SYMBOLS

The force- and moment-coefficient data are referenced to both the stability and body systems of axes. The coordinate origin was taken on the body axis of symmetry at a point 66.6 percent of the body length from the nose.

a   diameter of front face of theoretical cone frustum, in.

b   diameter of flat area on model nose, in.

c   longitudinal length of conical afterbody, in.

C_A axial-force coefficient, $\dfrac{\text{Axial force}}{q_{\infty}A}$

C_D drag coefficient, $\dfrac{\text{Drag}}{q_{\infty}A}$

C_L lift coefficient, $\dfrac{\text{Lift}}{q_{\infty}A}$

C_m pitching-moment coefficient, $\dfrac{\text{Pitching moment}}{q_{\infty}Ad}$

C_m/C_N longitudinal center-of-pressure location, fraction of base diameter d, from moment reference center

C_N normal-force coefficient, $\dfrac{\text{Normal force}}{q_\infty A}$

d   reference length (maximum diameter at base of cone), in.

L/D   lift-drag ratio, C_L/C_D

K   nose bluntness factor, b/a (fig. 1)

l length of model, nose to flat base (fig. 1), in.

M_∞ free-stream Mach number

q_∞ free-stream dynamic pressure, lb/sq in.

r   nose-edge radius, in.

R   radius of spherical base, 1.25d, in.

A   reference area, area of flat base, $\dfrac{\pi d^2}{4}$, sq in.

α angle of attack, deg

λ fineness ratio, l/d

θ cone semiangle, deg

MODELS

The geometrical description of a typical model is shown in figure 1 and the dimensions for the nine configurations tested are listed in table I. Photographs of the models are shown as figure 2. The configurations are identified by a four-digit code as follows:

(a) First digit gives nose-bluntness factor K:

First digit	K
1	0 (Spherical)
2	.50
3	.75

(b) Second digit gives fineness ratio λ:

Second digit	λ
1	0.50
2	.75
3	1.00

(c) Third digit gives cone semi-angle θ:

Third digit	θ, deg
1	10
2	15
3	20

(d) Fourth digit gives base shape:

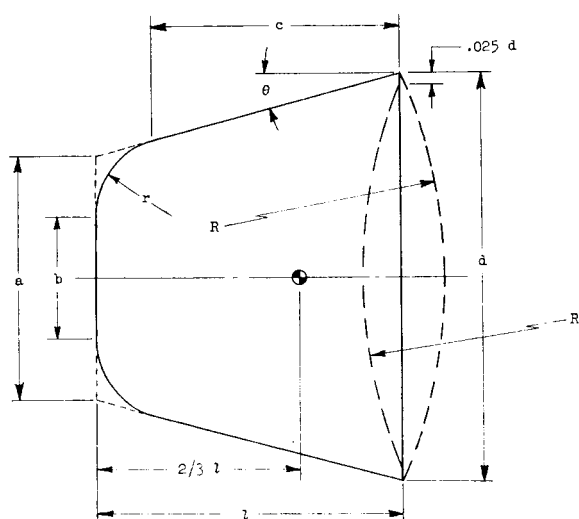| Fourth digit	Shape
1	Flat
2	Convex
3	Concave

Figure 1.- Sketch showing geometric parameters of planetary entry models.

Example: Configuration 1221 has a spherical nose, fineness ratio of 0.75, cone semiangle of 15°, and a flat base. For each configuration, there were two or three models which were identical in shape except for the position of the balance-mounting hole. (See fig. 3.) All models were made of polished stainless steel and had 4-inch-diameter bases, except configuration 1121 mounted at 90° to the sting. This particular model, used for tests at angles of attack from 44° to 137°, was a 1.5-scale model of the nose- and base-mounted models and was made of aluminum. (See fig. 2(b).) This larger size model of configuration 1121 was necessary to provide sufficient balance-mounting space.

The basic configuration was designated 1221. The variations from this configuration were: two flat-nosed configurations, 2221 and 3221; two different fineness-ratio configurations, 1121 and 1321; two different cone-semiangle configurations, 1211 and 1231; and two different base-shape configurations, 1222 and 1223. (See fig. 2.)

APPARATUS AND TESTS

The tests were made in the Langley transonic blowdown tunnel which has a slotted octagonal test section measuring 26 inches between flats. Model forces and moments were measured with a six-component internal strain-gage balance and recorded on pen-type strip recorders. The pressures necessary to determine dynamic pressure and Mach number were obtained on quick-response flight-type recorders.
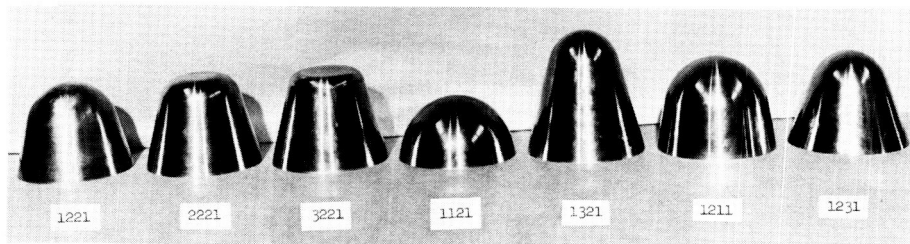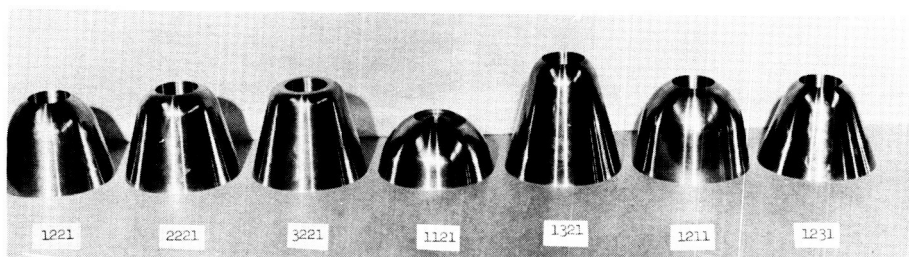
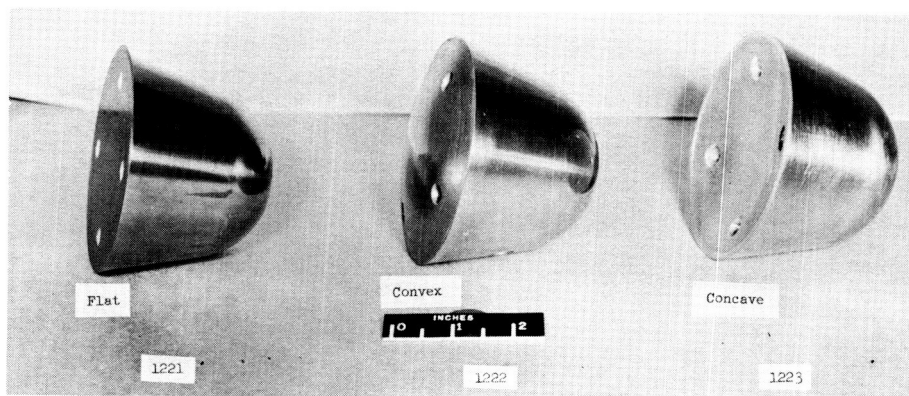(a) Base-mounted models ($-1^{\circ} \leqq \alpha \leqq 47^{\circ}$).   L-62-6092
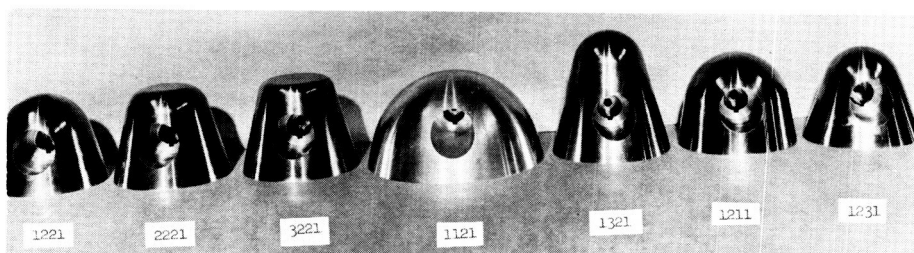
(b) Top-mounted models ($44^{\circ} \leqq \alpha \leqq 137^{\circ}$).   L-62-6093

(c) Nose-mounted models ($134^{\circ} \leqq \alpha \leqq 180^{\circ}$).   L-62-6090

(d) Base shapes.   L-62-6091

Figure 2.- Photographs of models showing shapes and mounting holes.

TABLE I.- GEOMETRIC PARAMETERS OF LOW-FINENESS-RATIO

BLUNTED-CONE PLANETARY-ENTRY MODELS

Configuration code	a, in.	b, in.	l, in.	d, in.	c, in.	*r, in.	θ, deg	Base
1221	2.392	0	3	4	1.845	1.559	15	Flat
2221	2.392	1.196	3	4	2.423	.779	15	Flat
3221	2.392	1.794	3	4	2.711	.390	15	Flat
1121	2.928	0	2	4	.587	1.907	15	Flat
1121 (large)	4.392	0	3	6	.880	2.861	15	Flat
1321	1.856	0	4	4	3.103	1.210	15	Flat
1211	2.942	0	3	4	1.550	1.753	10	Flat
1231	1.816	0	3	4	2.147	1.297	20	Flat
1222	2.392	0	3	4	1.845	1.559	15	Convex (R = 5 in.)
1223	2.392	0	3	4	1.845	1.559	15	Concave (R = 5 in.)

*Spherical when b equals zero.
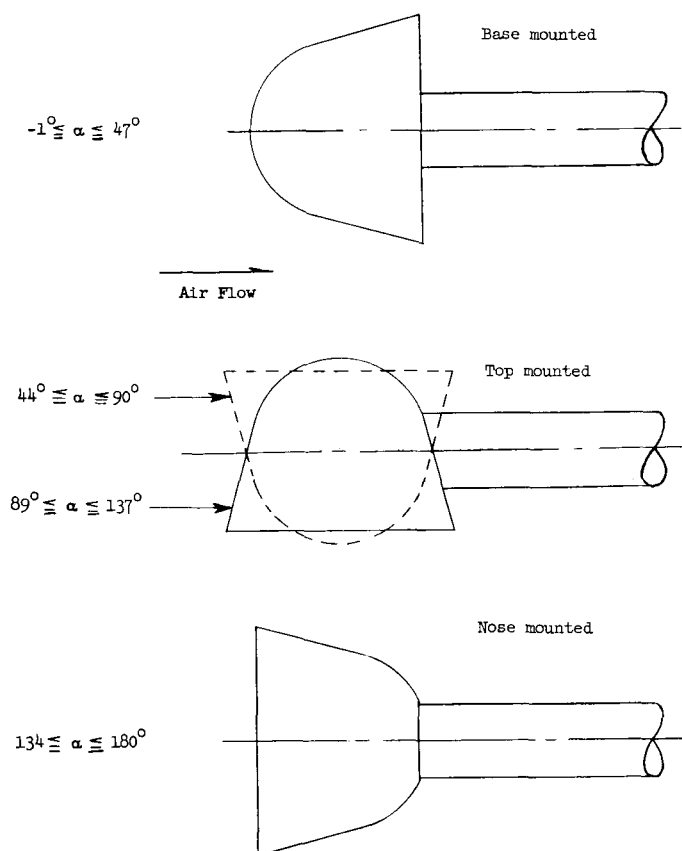
Figure 3.- Sketch showing typical model in the four mounting positions for the different angle-of-attack ranges.

Balance angles of attack from 0° to 21° and from 25° to 45° were obtained with a straight sting and a 25° bent sting, respectively. The model angle-of-attack range of 0° to 180° was obtained by mounting the models at 0°, 90°, and 180° relative to the longitudinal axis of the balance. (See fig. 3.) Table II indicates the sting used and the model-mounting position for each angle-of-attack range. For these sting and model combinations, the model angle of attack was always increased positively during each test run. Data were obtained for each configuration at about 3° increments for angles of attack from 0° to 21° and in 5° increments for angles of attack from 25° to 180°. The convex- and concave-base configurations and the two flat-nose configurations were not tested at angles of attack from 0° to 45° and from 135° to 180°, respectively. For these angles of attack, the effect of base shape or nose shape on the static longitudinal aerodynamic characteristics was believed to be negligible.

The basic configuration 1221 was tested at nominal Mach numbers of

0.80, 0.90, 0.95, 1.00, and 1.20. The other configurations were tested at nominal Mach numbers of 0.80 and 1.20 only. The Mach numbers are referred to as nominal because the Mach numbers varied with angle of attack. This variation was due to the fact that the tunnel was operated at a constant stagnation pressure and the tunnel blockage caused by the sting support, sting, and model varied with angle of attack. Measured Mach numbers at the beginning and end of each angle-of-attack range are given in table III. Stagnation pressure was held at 35 pounds per square inch absolute, except for a few runs on the 1.5-scale model of configuration 1121, which were made at a stagnation pressure of 30 pounds per square inch absolute to reduce the balance loads and to keep the Reynolds number approximately the same as that of the smaller models. The Reynolds number for the tests, based on the base diameter, varied from 3.67×10^6 to 5.32×10^6. Calculations using the method of reference 6 indicated that the wall-reflected bow shock would clear the models.

TABLE II.- STING AND MODEL-MOUNTING POSITION

Angle-of-attack range, deg	Sting angle, deg	Model-mounting position
0 to 21 25 to 45	0 25 (bent)	0° to balance (base mounted)
44 to 65 69 to 90 90 to 111 115 to 135	25 (bent) 0 0 25 (bent)	90° to balance (top mounted)
134 to 155 159 to 180	25 (bent) 0	180° to balance (nose mounted)

TABLE III.- TEST MACH NUMBERS AT FIRST AND LAST TEST POINTS IN ANGLE-OF-ATTACK RANGE

Configuration	Nominal M_∞	First and last value of M_∞ in α ranges between –								Average M_∞
		-1°, 21°	25°, 47°	44°, 65°	69°, 90°	89°, 111°	115°, 137°	134°, 155°	160°, 180°	
1221	0.80	0.79, 0.79	0.82, 0.81	0.82, 0.81	0.81, 0.81	0.81, 0.80	0.83, 0.83	0.81, 0.82	0.82, 0.81	0.81
	.90	.90, .87	.91, .89	.91, .93	.90, .89	.91, .89	.93, .92	.91, .90	.91, .89	.90
	.95	.94, .93	.97, .95	.96, .97	.95, .96	.96, .95	.98, .96	.96, .95	.98, .95	.96
	1.00	.98, .97	1.03, .99	1.01, 1.01	1.00, 1.03	1.02, 1.01	1.03, 1.01	1.01, 1.01	1.03, 1.00	1.00
	1.20	1.20, 1.20	1.21, 1.20	1.21, 1.22	1.19, 1.20	1.20, 1.20	1.24, 1.22	1.21, 1.21	1.21, 1.20	1.21
2221	.80	.80, .79	.82, .82	.83, .83	.82, .81	.82, .81	.84, .83	----------	----------	.82
	1.20	1.20, 1.19	1.22, 1.20	1.21, 1.22	1.20, 1.20	1.21, 1.22	1.22, 1.21	----------	----------	1.21
3221	.80	.80, .80	.82, .81	.82, .82	.82, .82	.83, .82	.83, .84	----------	----------	.82
	1.20	1.21, 1.19	1.22, 1.21	1.21, 1.22	1.21, 1.22	1.22, 1.21	1.23, 1.22	----------	----------	1.21
1121	.80	.80, .79	.82, .81	.81, .82	.80, .80	.82, .81	.83, .82	.81, .81	.83, .82	.81
	1.20	1.20, 1.19	1.20, 1.19	1.21, 1.23	1.22, 1.25	1.23, 1.21	1.21, 1.17	1.21, 1.18	1.22, 1.20	1.21
1321	.80	.80, .79	.82, .81	.83, .84	.81, .80	.82, .80	.84, .82	.82, .81	.83, .82	.81
	1.20	1.20, 1.20	1.21, 1.18	1.21, 1.21	1.22, 1.22	1.23, 1.23	1.23, 1.21	1.21, 1.21	1.22, 1.20	1.21
1211	.80	.80, .78	.82, .81	.83, .84	.81, .80	.81, .81	.83, .84	.82, .82	.83, .82	.81
	1.20	1.18, 1.17	1.20, 1.19	1.21, 1.22	1.19, 1.21	1.22, 1.22	1.21, 1.20	1.21, 1.20	1.22, 1.20	1.20
1231	.80	.80, .79	.83, .82	.83, .83	.82, .82	.81, .81	.83, .82	.82, .81	.82, .81	.81
	1.20	1.18, 1.20	1.22, 1.21	1.22, 1.23	1.20, 1.20	1.22, 1.22	1.23, 1.21	1.22, 1.20	1.22, 1.19	1.21
1222	.80	----------	----------	.84, .83	.82, .81	.80, .80	.84, .83	.82, .81	.82, .82	.82
	1.20	----------	----------	1.21, 1.22	1.20, 1.20	1.20, 1.19	1.23, 1.21	1.22, 1.21	1.23, 1.21	1.21
1223	.80	----------	----------	.83, .84	.81, .81	.81, .80	.84, .83	.82, .81	.83, .81	.82
	1.20	----------	----------	1.21, 1.22	1.20, 1.20	1.21, 1.20	1.23, 1.21	1.21, 1.20	1.22, 1.19	1.21

CORRECTIONS AND ACCURACY

The data of these tests have not been corrected for either tunnel-blockage effects or sting-interference effects. The axial-force data have not been adjusted to a condition of free-stream static pressure at the model base. The angle of attack has been corrected for sting and balance deflections due to aerodynamic loads.

Based upon balance accuracy, the maximum values of random errors in the body force and moment coefficients are:

$$\Delta C_N = \pm 0.01$$

$$\Delta C_A = \pm 0.01$$

$$\Delta C_m = \pm 0.008$$

The estimated accuracies of Mach number and angle of attack are:

$$\Delta M_\infty = \pm 0.01$$

$$\Delta \alpha = \pm 0.1^\circ$$

PRESENTATION OF RESULTS

The effects of variations in Mach number on the static longitudinal aerodynamic characteristics of the basic configuration 1221 are presented in figure 4. The effect of variations in nose bluntness on the static longitudinal aerodynamic characteristics of the basic configuration at Mach numbers of 0.8 and 1.2 is shown in figures 5 and 6, respectively. In like manner, figures 7 and 8 present the data for varied fineness ratio, figures 9 and 10 for cone semiangle variations, and figures 11 and 12 for base-shape variations. The effect of moment-reference-center location on the variation of pitching-moment coefficient with angle of attack for configuration 1221 at Mach numbers of 0.8 and 1.2 is shown in figure 13.

DISCUSSION

In some cases, the data for adjacent angle-of-attack ranges are not continuous. Such discontinuities occur mainly at 45° and 135° angle of attack and are due primarily to differences in the position of the sting relative to the model. (See fig. 3.) Discontinuities at angles of attack other than 45° and 135° are

most likely due to a difference in Mach number between the last data point on one angle-of-attack range and the first data point on the next. (See table III.)

Effect of Mach Number

With the exception of pitching-moment coefficient, variations in Mach number changed the absolute magnitudes of the aerodynamic coefficients of the basic configuration 1121 (fig. 4). Variations in Mach number had essentially no effect on pitching-moment coefficient. For the assumed moment reference center, this configuration is slightly unstable up to an angle of attack of about 15° and unstable from an angle of attack of about 90° to 150°. The configuration is stable at angles of attack from about 15° to 90° and from about 150° to 180°. The stable trim point at 180° angle of attack is clearly undesirable for a ballistic body intended to maintain a constant nose-forward orientation throughout its reentry trajectory.

Effect of Nose Bluntness

The data of figures 5 and 6 at nominal Mach numbers of 0.8 and 1.2, respectively, show that the present type of variation in nose bluntness had no significant effects on the static longitudinal aerodynamic characteristics.

Effect of Fineness Ratio

The effects of variations in fineness ratio on the static longitudinal aerodynamic characteristics are shown in figures 7 and 8 at nominal Mach numbers of 0.8 and 1.2, respectively. A trend of decreasing stability with increasing fineness ratio is noted at both Mach numbers at angles of attack from about 0° to 45° with the lowest-fineness-ratio body ($\lambda = 0.5$) the only one of the three tested that was stable near $\alpha = 0°$. At angles of attack up to about 45°, the longitudinal center-of-pressure location apparently tends to remain near the center of the spherical nose for the various fineness ratios whereas the assumed moment reference center, at two-thirds of the model length from the nose, has a relative rearward movement with increased fineness ratio. Fineness ratio had no effect on the undesirable stable slope of pitching-moment curves near an angle of attack of 180°.

Generally, increases in fineness ratio caused large increases in normal-force coefficient at both test Mach numbers through most of the angle-of-attack range. These increases are associated with the increase in planform area resulting from increased fineness ratio. The ratios of planform area to reference area for configurations 1121, 1221, and 1321 are 0.41, 0.67, and 0.88, respectively. As expected, however, little effect of fineness ratio on normal-force coefficient was noted at angles of attack near 0° or near 180°.

Increases in fineness ratio caused reductions in the absolute values of axial-force coefficient at angles of attack up to about 75° and between 90° and 155°. Generally, these reductions in C_A were larger for an increase in fineness ratio from $\lambda = 0.50$ to 0.75 than for the increase from $\lambda = 0.75$ to 1.00.

9

Effects of Cone Semiangle

The effects of variations in cone semiangle on the longitudinal aerodynamic characteristics of a blunted cone are shown in figures 9 and 10 for Mach numbers of 0.8 and 1.2, respectively. Variations in cone semiangle had no significant effects on the longitudinal stability at the two test Mach numbers.

Increases in cone semiangle caused decreases in normal-force coefficient at angles of attack up to about 35° (figs. 9(b) and 10(b)). Above this angle of attack, increases in cone semiangle had little or no effect on C_N at Mach number 0.8 (fig. 9(b)) but caused decreases in normal-force coefficient at Mach number 1.2 at angles of attack up to 150° (fig. 10(b)).

Except for angles of attack near 0° at both test Mach numbers and near 90° at M = 0.8, the effect of variations in cone semiangle on C_A was generally small (figs. 9(b) and 10(b)).

Effect of Variations in Base Shape

The data of figures 11(a) and 12(a) show no significant effect of variations in base shape on the static longitudinal stability although at angles of attack between 80° and 140°, variations in base shape did cause some differences in the values of pitching-moment coefficient for a given angle of attack. The present variations in base shape had essentially no effect on normal-force coefficient throughout the entire test angle-of-attack range or on axial-force coefficient at angles of attack up to about 80°. (See figs. 11(b) and 12(b).) Above 80° angle of attack, variations in base shape had a considerable effect on axial-force coefficient. From angles of attack of 80° to 180°, the absolute value of C_A is, in general, higher for the concave-base configuration than for the convex base, with the absolute values of C_A for the flat-base configuration occurring between these values.

Effect of Moment-Reference-Center Location

The pitching-moment data of figures 4(a) through 12(a) indicate that variations in Mach number, nose shape, fineness ratio, cone semiangle, and base shape had a negligible effect on the stable trim point at an angle of attack of 180°. The moment-reference center for these data was located at two-thirds of the body length from the nose. The variation of C_m with α was recalculated for configuration 1221 for moment-reference-center locations of 58 and 50 percent of the model length from the nose at the nominal Mach numbers of 0.8 and 1.2. As shown in figure 13, forward movement of the moment-reference center increased the stability near 0° angle of attack and caused negative increments in pitching-moment coefficient at angles of attack up to about 150°. Above an angle of attack of 150°, however, moment-reference-center location has no significant effect on pitching moment because the normal-force coefficient in this angle-of-attack range is almost zero for all test Mach numbers (fig. 4(b)). It is clear that no moment-reference-center shift would affect the pitching moment near 180° for any of the

configurations tested, since all models tested at all test Mach numbers have values of C_N near zero above an angle of attack of about 150°. All configurations tested had a stable trim point at an angle of attack of 180°; such a trim point is undesirable for a passive entry body from a static stability standpoint if nose-forward entry is intended.

CONCLUSIONS

An investigation has been conducted in the Langley transonic blowdown tunnel to determine the effects of variations in Mach number, nose bluntness, fineness ratio, cone semiangle, and base shape on the static longitudinal aerodynamic characteristics of low-fineness-ratio blunted cones. The tests were made at Mach numbers from about 0.8 to 1.2 through an angle-of-attack range that generally varied from 0° to 180°. Reynolds number, based upon the base diameter, varied from 3.67×10^6 to 5.32×10^6.

The results of the investigation indicate the following:

1. The configurations of the present investigation all have a stable trim point at an angle of attack of 180°, which is undesirable from a static stability standpoint for a passive entry body if nose-forward entry is intended.

2. Variations in Mach number, nose bluntness, cone semiangle, and base shape had no significant effect on the static stability but increases in fineness ratio caused decreases in stability at angles of attack up to 45° with the moment-reference center located two-thirds of the body length from the nose.

3. Increases in fineness ratio and decreases in cone semiangle generally caused an increase in normal-force coefficient over most of the test angle-of-attack range. Variations in nose bluntness and base shape had little or no effect on normal-force coefficient.

4. At angles of attack up to about 160°, increases in fineness ratio generally caused a reduction in the absolute values of axial-force coefficient. The effect of variations in cone semiangle on axial-force coefficient was generally small, except for angles of attack near 0° at both test Mach numbers and near 90° at Mach number 0.8. Variations in nose bluntness and base shape at angles of attack below 80° had little or no effect on axial-force coeffcient. However, variations in base shape had considerable effect on axial-force coefficient at angles of attack above 80°. The variation in base shape from convex to concave caused, in general, a large increase in the absolute value of axial-force coefficient at angles of attack from 80° to 180°.

Langley Research Center,
        National Aeronautics and Space Administration,
            Langley Station, Hampton, Va., April 30, 1963.

REFERENCES

1. Shaw, David S., Fuller, Dennis E., and Babb, C. Donald: Effects of Nose Bluntness, Fineness Ratio, Cone Angle, and Model Base on the Static Aerodynamic Characteristics of Blunt Bodies at Mach Numbers of 1.57, 1.80, and 2.16 and Angles of Attack Up to 180°. NASA TN D-1781, 1963.

2. Treon, Stuart L.: Static Aerodynamic Characteristics of Short Blunt Cones With Various Nose and Base Cone Angles at Mach Numbers From 0.6 to 5.5 and Angles of Attack to 180°. NASA TN D-1327, 1962.

3. Treon, Stuart L.: The Effect of Nose Shape on the Static Aerodynamic Characteristics of Ballistic-Type Missile Models at Mach Numbers From 0.6 to 1.4. NASA MEMO 5-17-59A, 1959.

4. Fisher, Lewis R., Keith, Arvid L., Jr., and DiCamillo, Joseph R.: Aerodynamic Characteristics of Some Families of Blunt Bodies at Transonic Speeds. NASA MEMO 10-28-58L, 1958.

5. Reese, David E., Jr., and Wehrend, William R., Jr.: An Investigation of the Static and Dynamic Aerodynamic Characteristics of a Series of Blunt-Nosed Cylinder-Flare Models at Mach Numbers From 0.65 to 2.20. NASA TM X-110, 1960.

6. Moeckel, W. E.: Approximate Method for Predicting Form and Location of Detached Shock Waves Ahead of Plane or Axially Symmetric Bodies. NACA TN 1921, 1949.
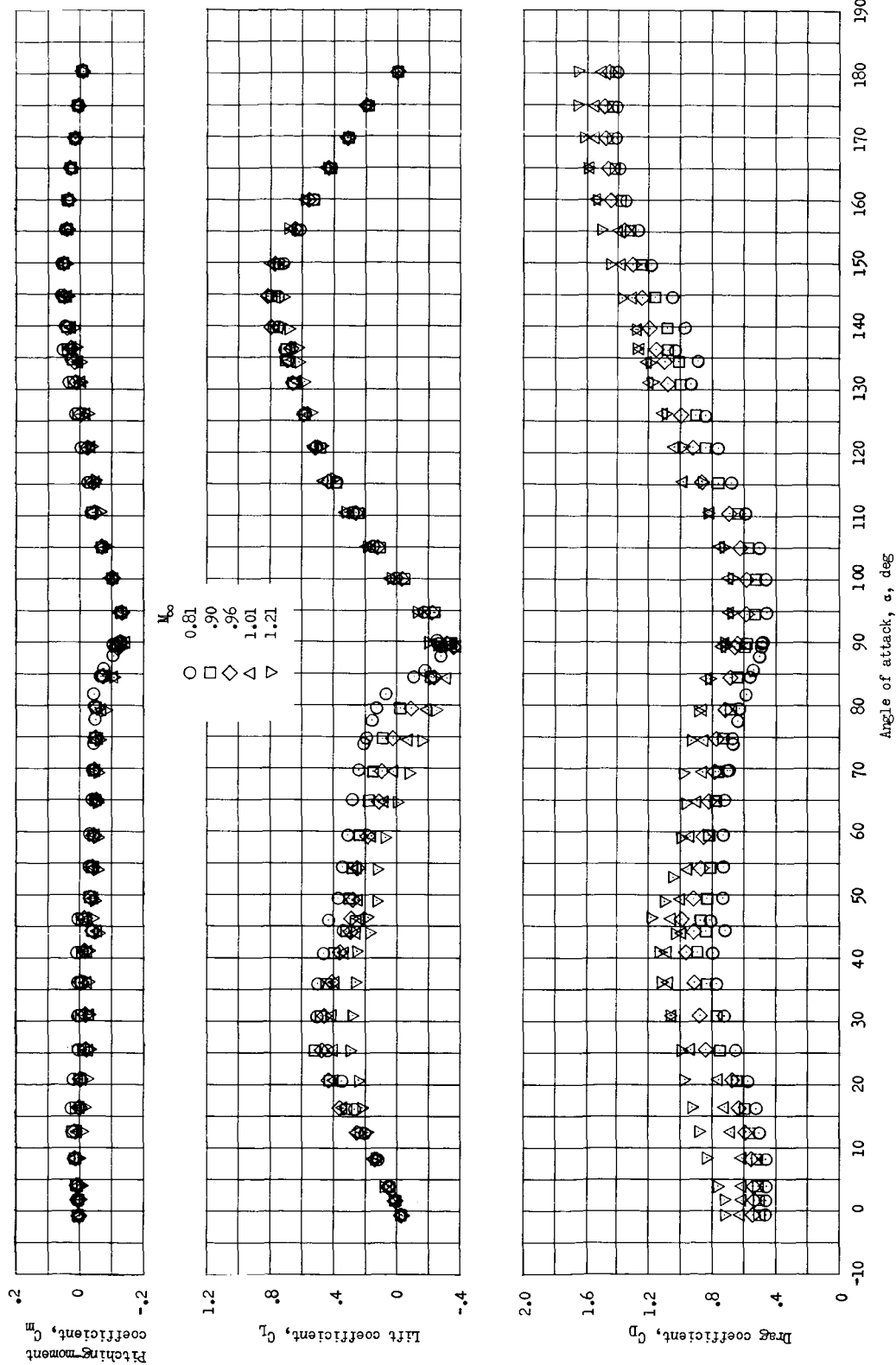
(a) Variation of C_m, C_L, and C_D with α.

Figure 4.- Effect of variations in Mach number on the longitudinal aerodynamic characteristics of a flat-base blunted cone with spherical nose, fineness ratio of 0.75, and cone semiangle of 15°. Configuration 1221.

13
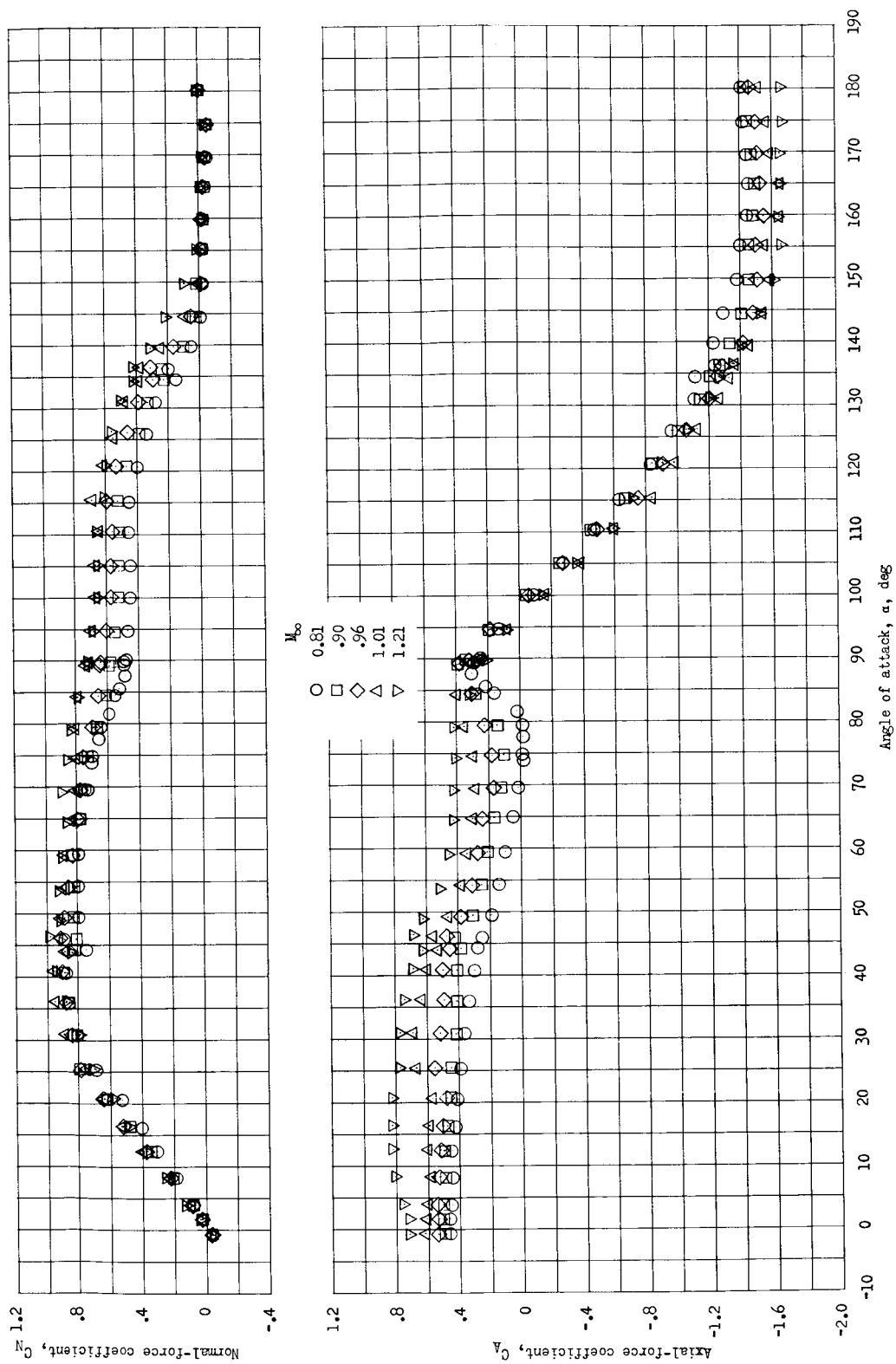
(b) Variation of C_N and C_A with α.

Figure 4.- Continued.
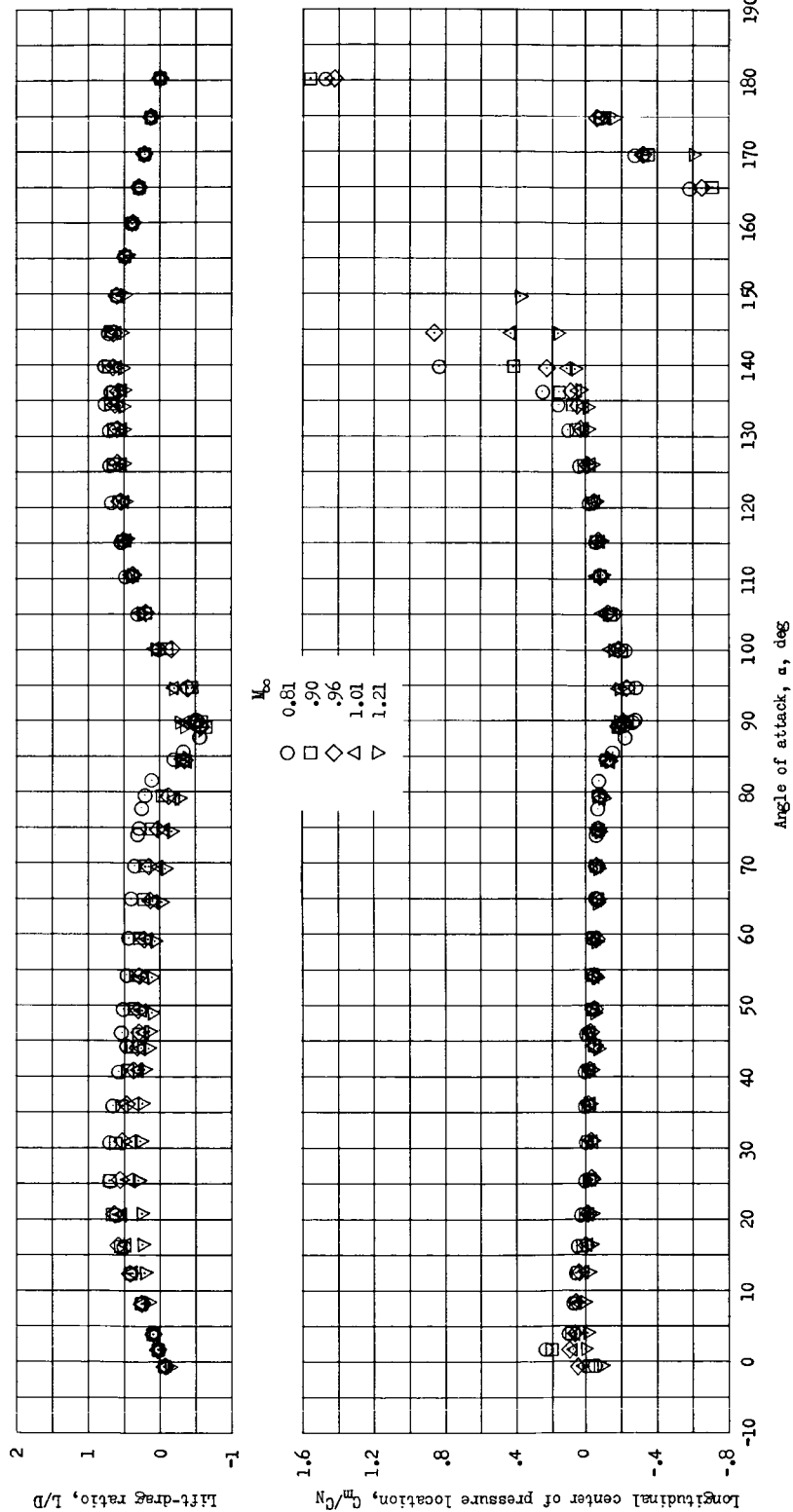
(c) Variation of L/D and C_m/C_N with α.

Figure 4.- Concluded.
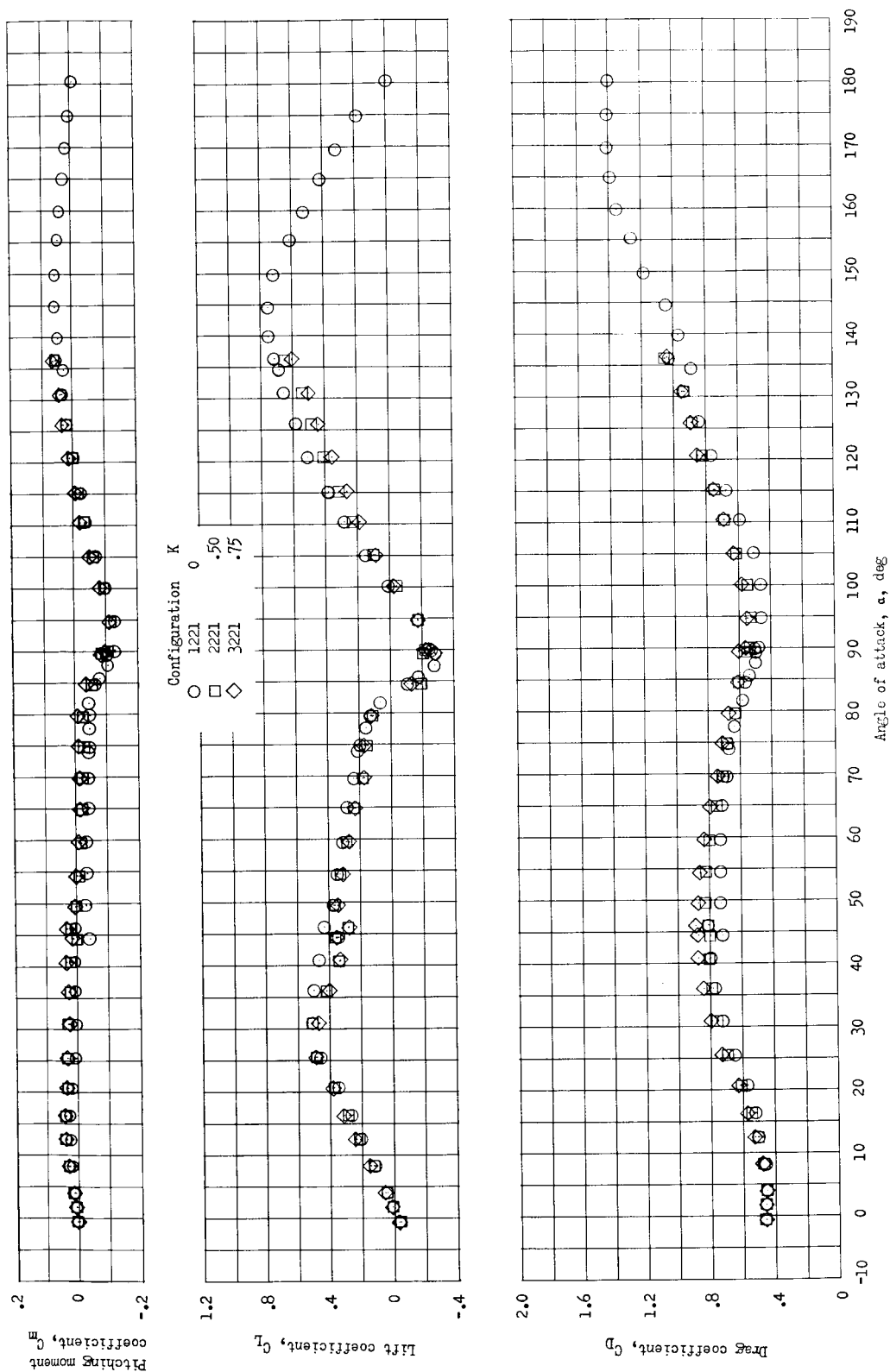
(a) Variation of C_m, C_L, and C_D with α.

Figure 5.- Effect of variations in nose shape on the longitudinal aerodynamic characteristics of a flat-base blunted cone with fineness ratio of 0.75 and cone semiangle of 15°. Nominal $M_\infty = 0.8$.
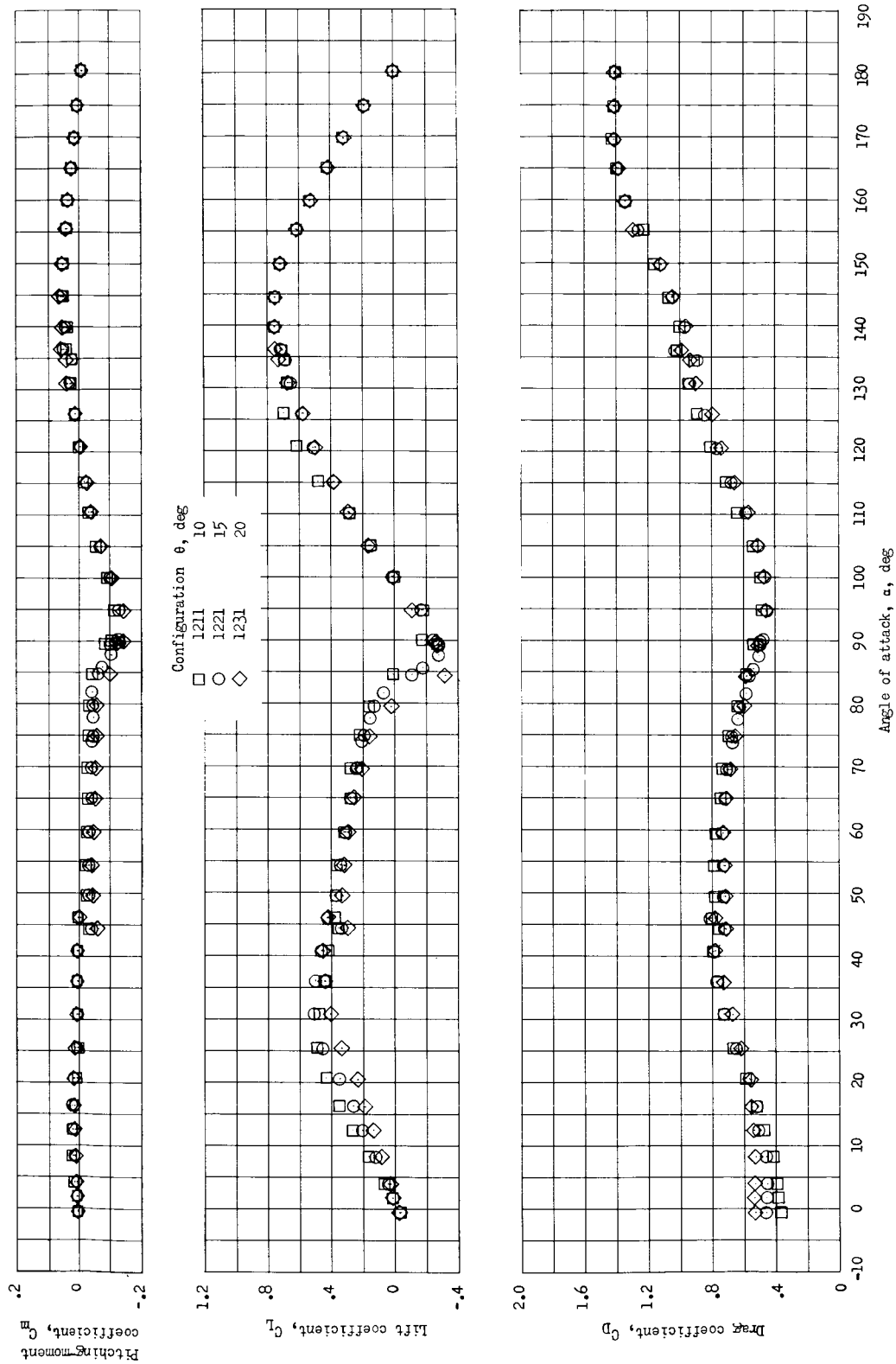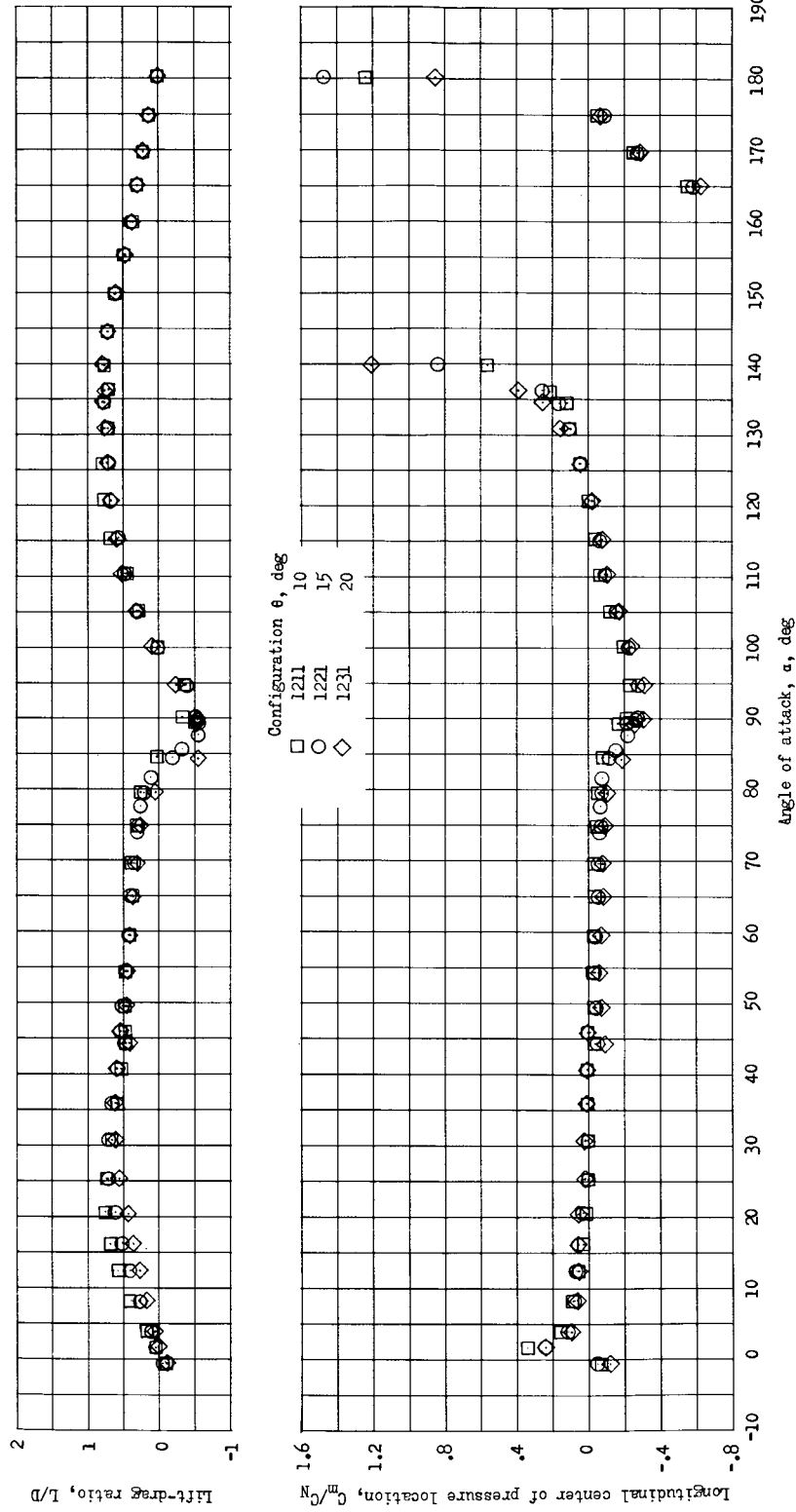
16
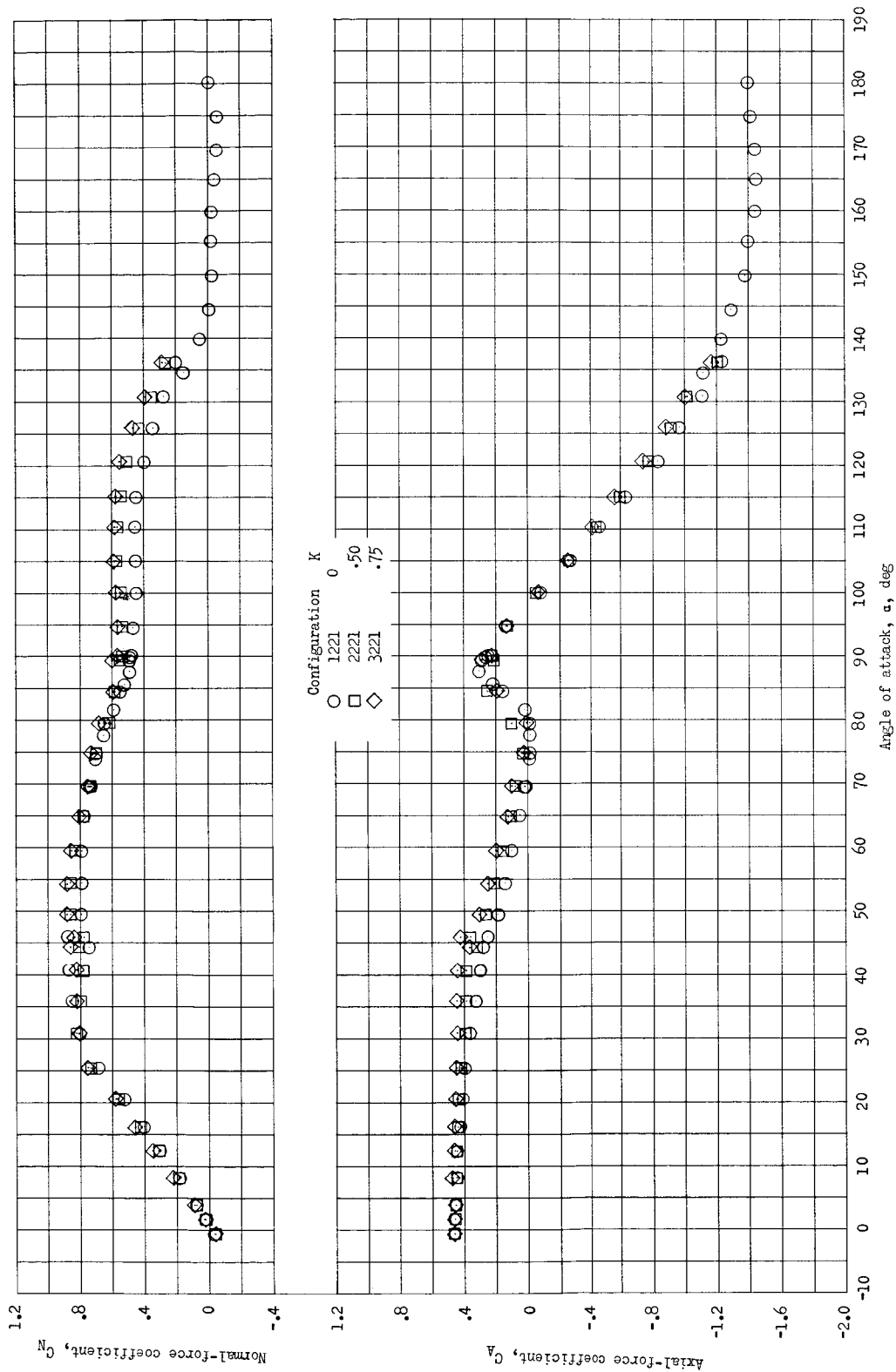
(b) Variation of C_N and C_A with α.

Figure 5.- Continued.
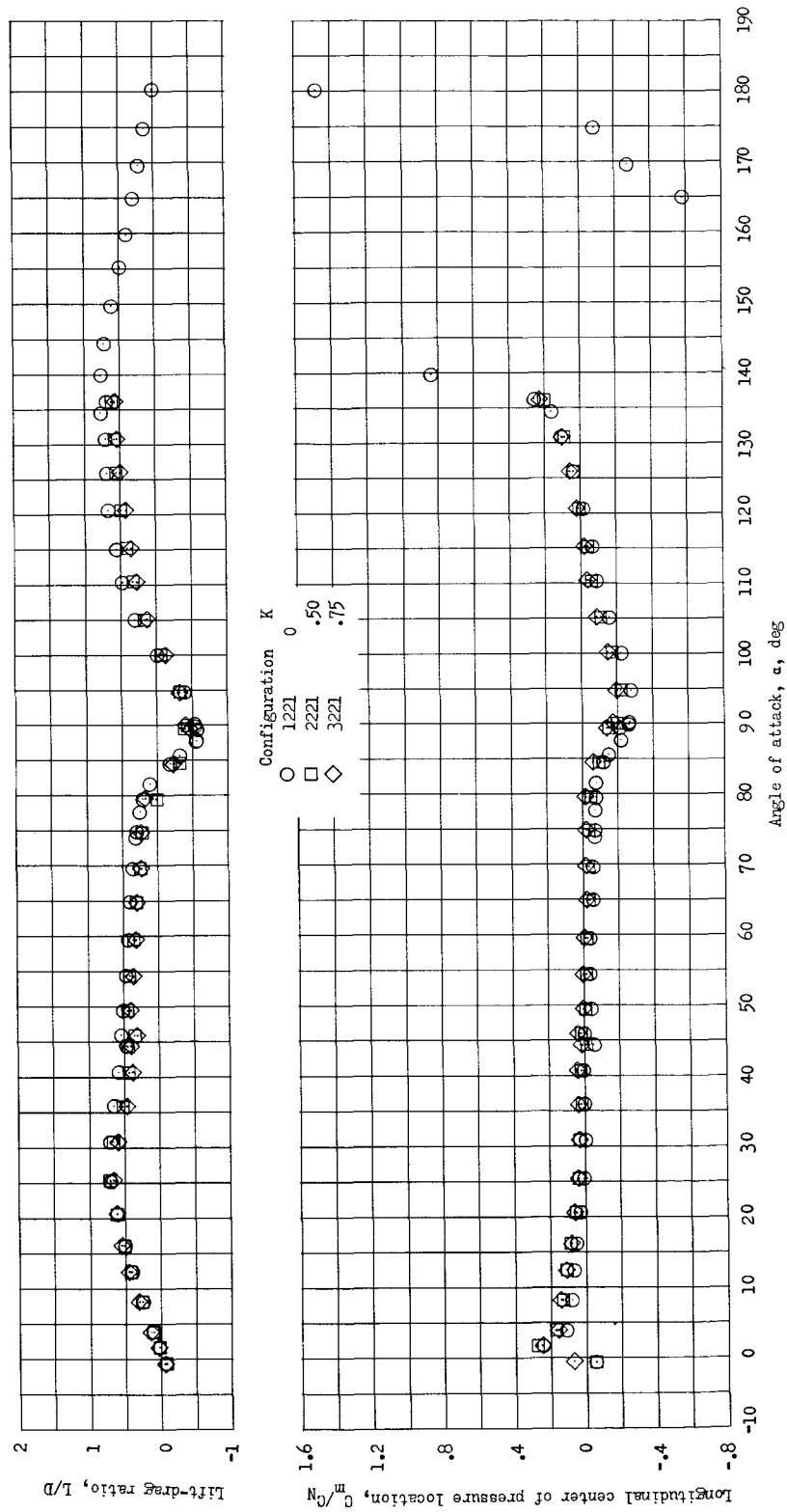
(c) Variation of L/D and C_m/C_N with α.

Figure 5.- Concluded.
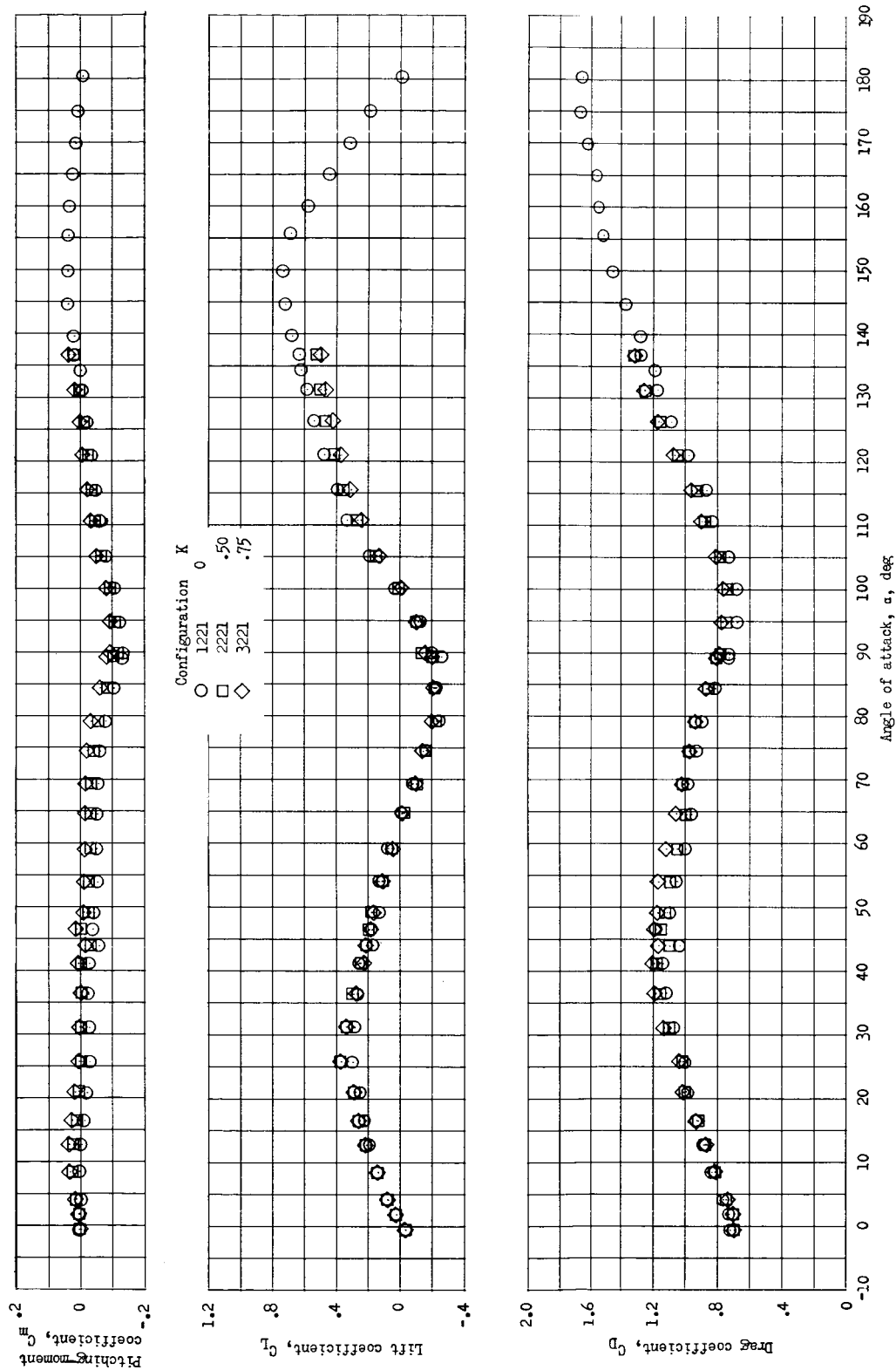
Figure 6.- Effect of variations in nose bluntness on the longitudinal aerodynamic characteristics of a flat-base blunted cone with fineness ratio of 0.75 and cone semiangle of 15°. Nominal M_∞ = 1.2.

(a) Variation of C_m, C_L, and C_D with α.

19
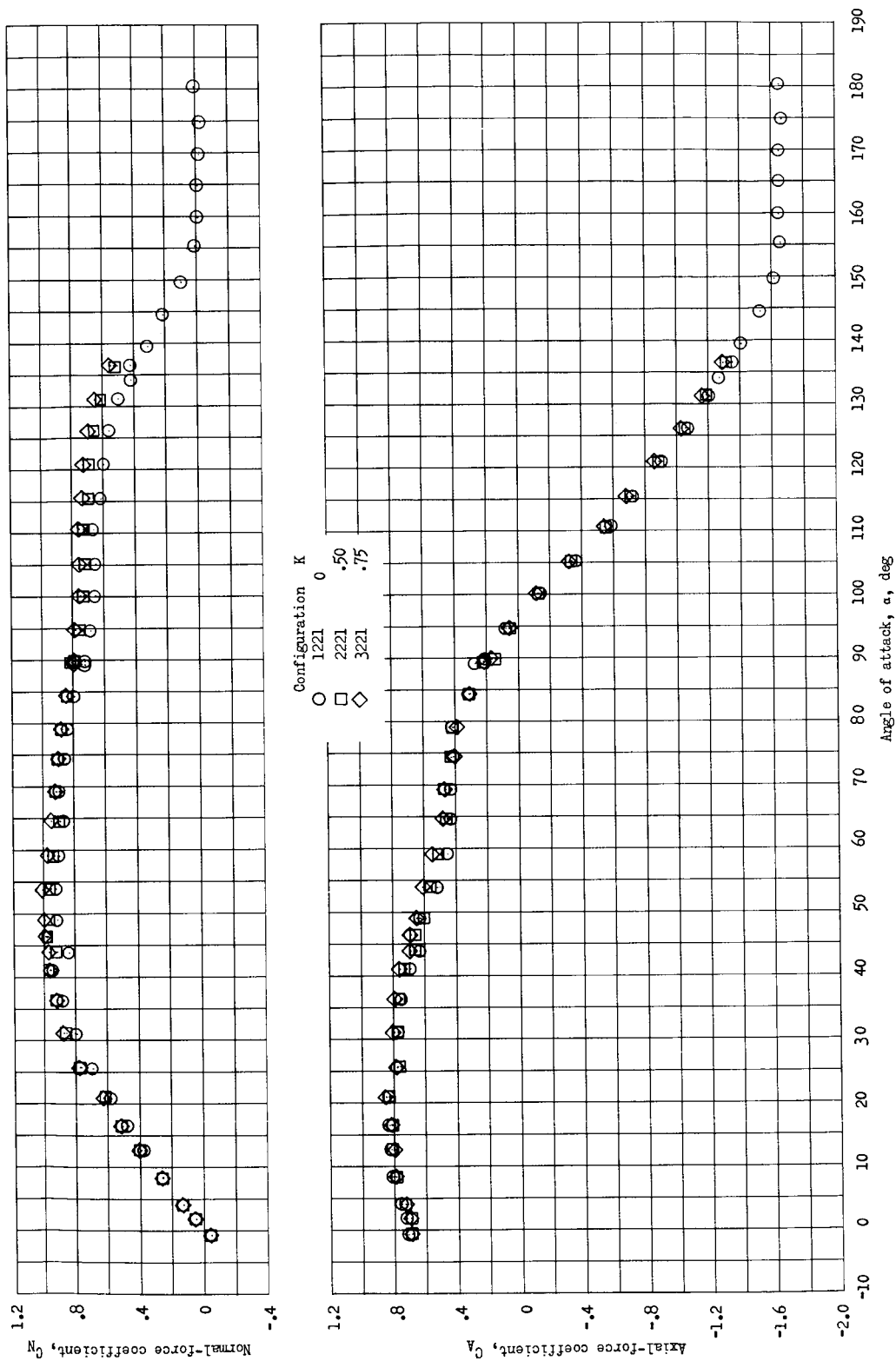
(b) Variation of C_N and C_A with α.

Figure 6.- Continued.
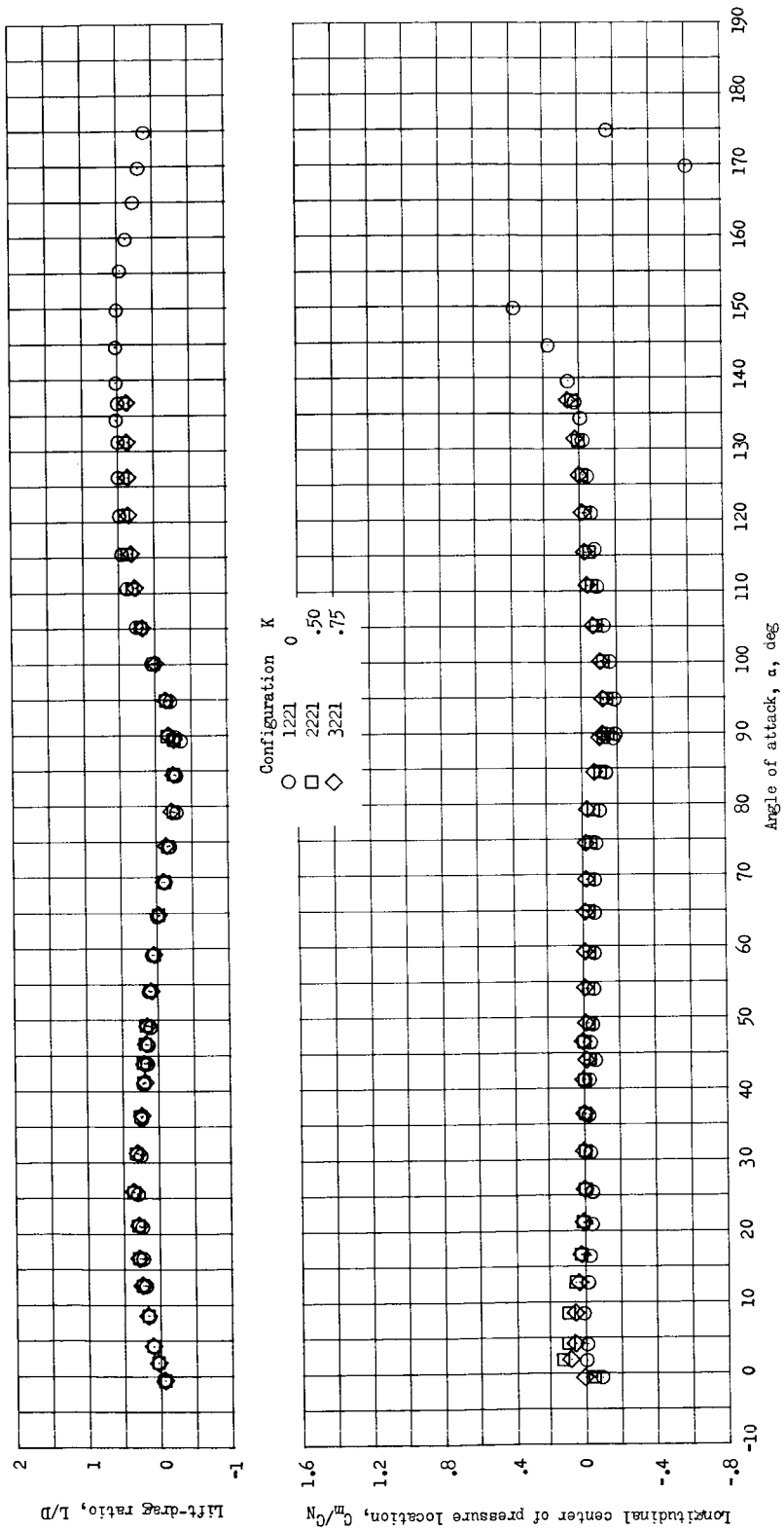
(c) Variation of L/D and C_m/C_N with α.

Figure 6.- Concluded.
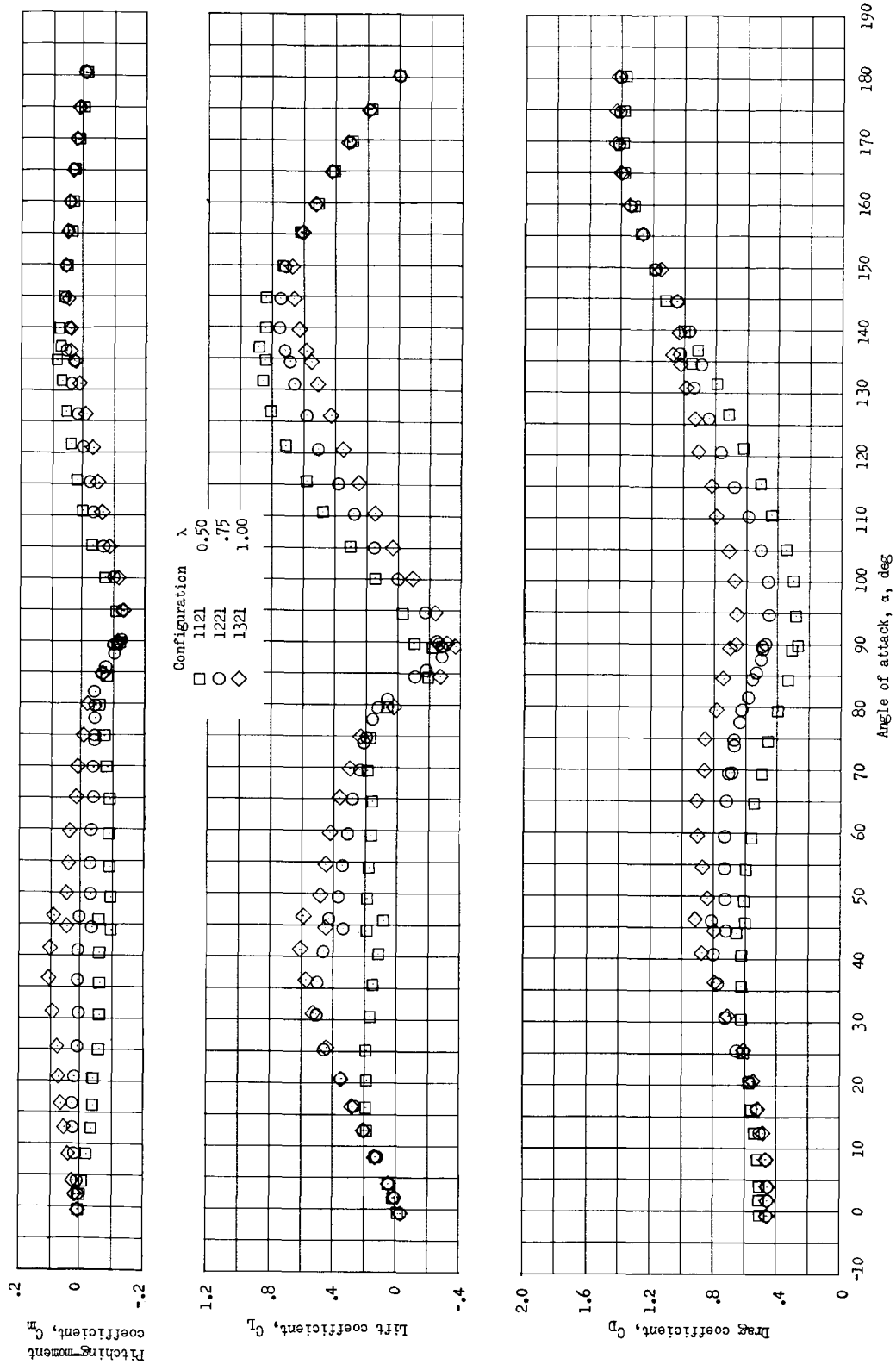
(a) Variation of C_m, C_L, and C_D with α.

Figure 7.- Effect of variations in fineness ratio on the longitudinal aerodynamic characteristics of a flat-base blunted cone with spherical nose and cone semiangle of 15°. Nominal $M_\infty = 0.8$.
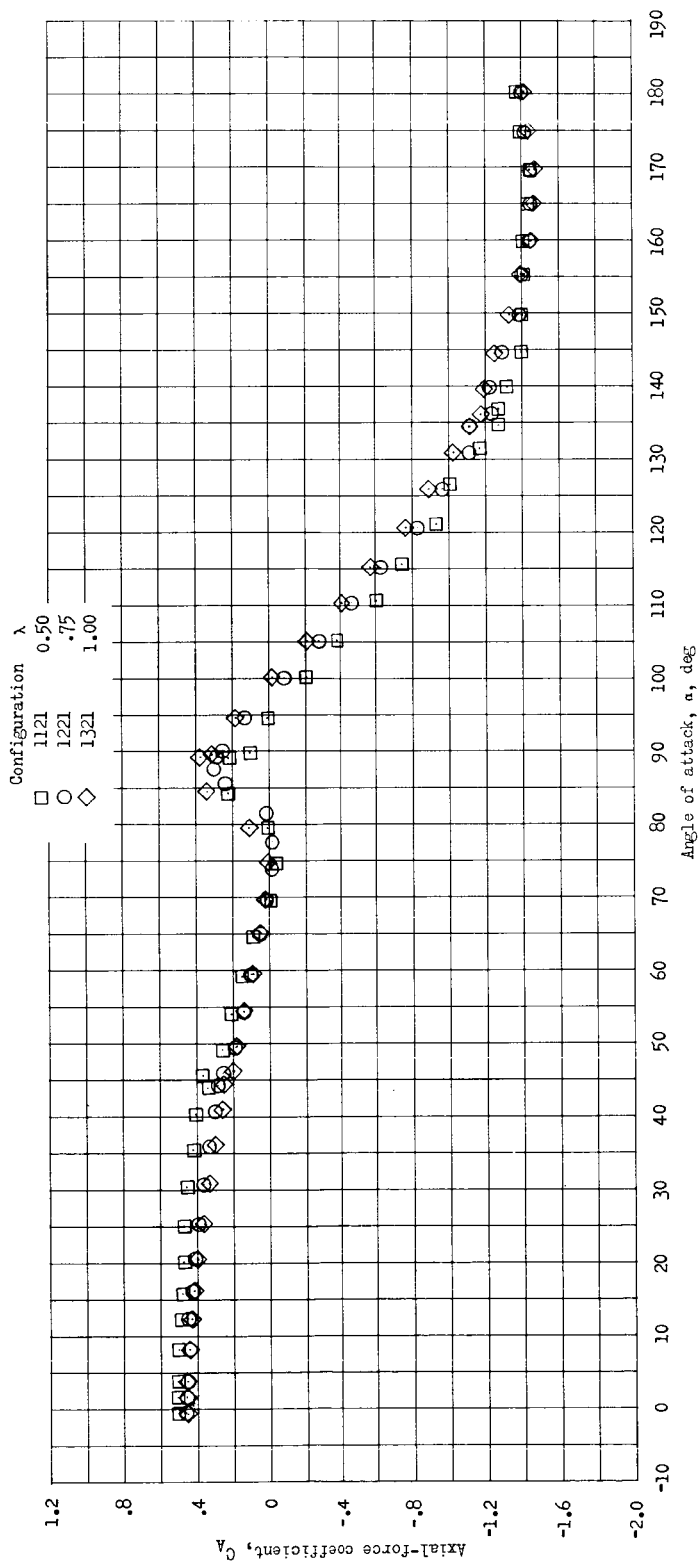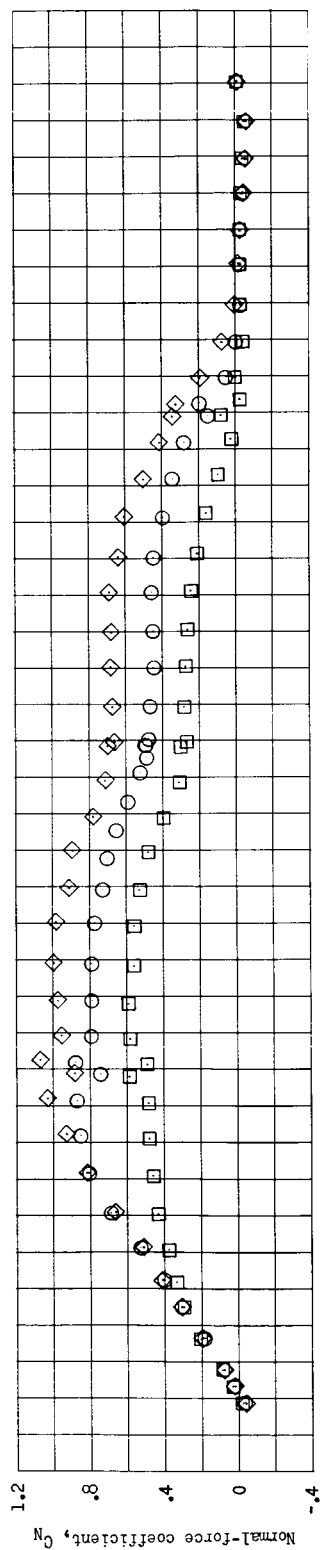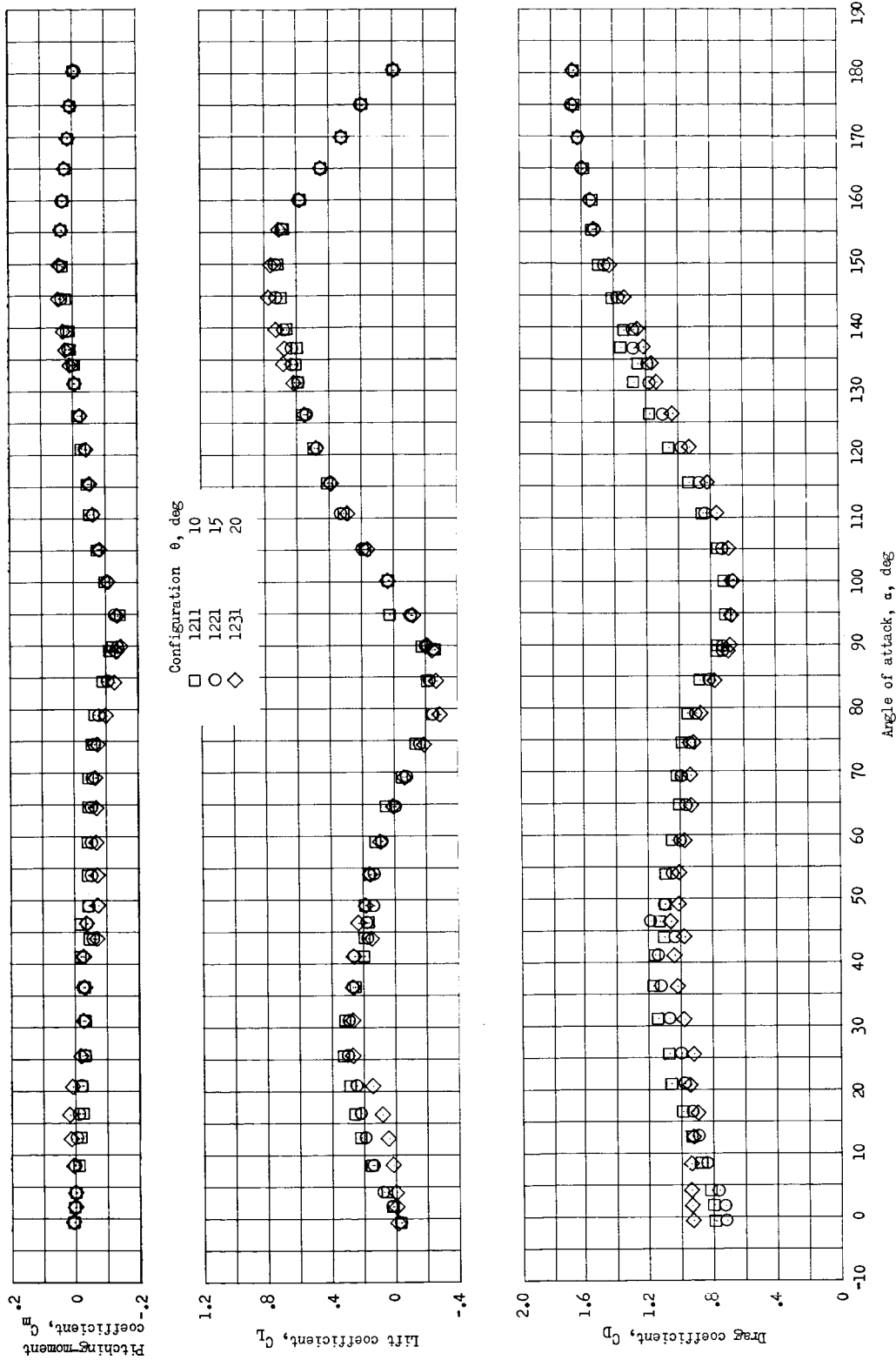
(b) Variation of C_N and C_A with α.

Figure 7.- Continued.
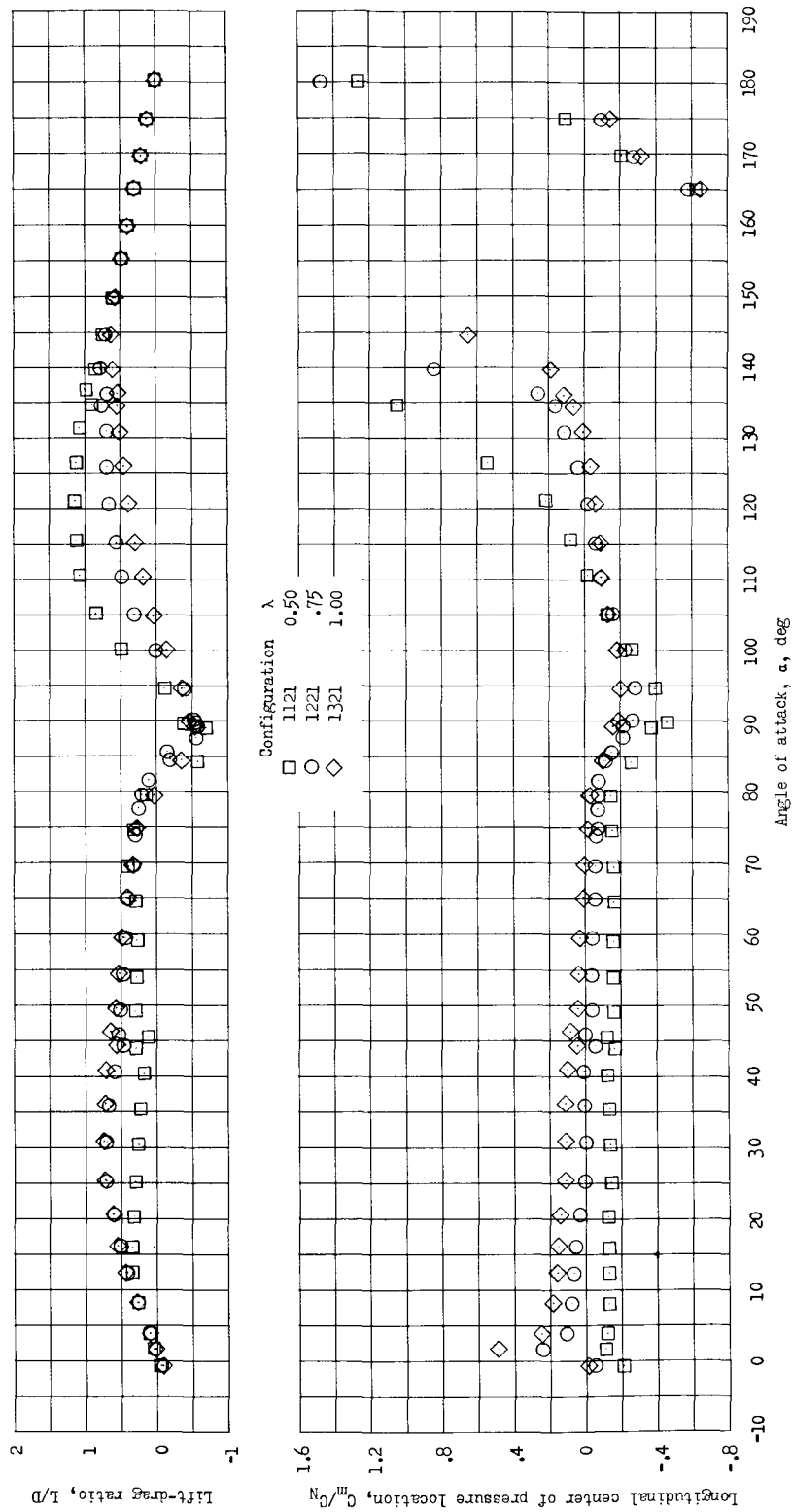
(c) Variation of L/D and C_m/C_N with α.

Figure 7.- Concluded.

24
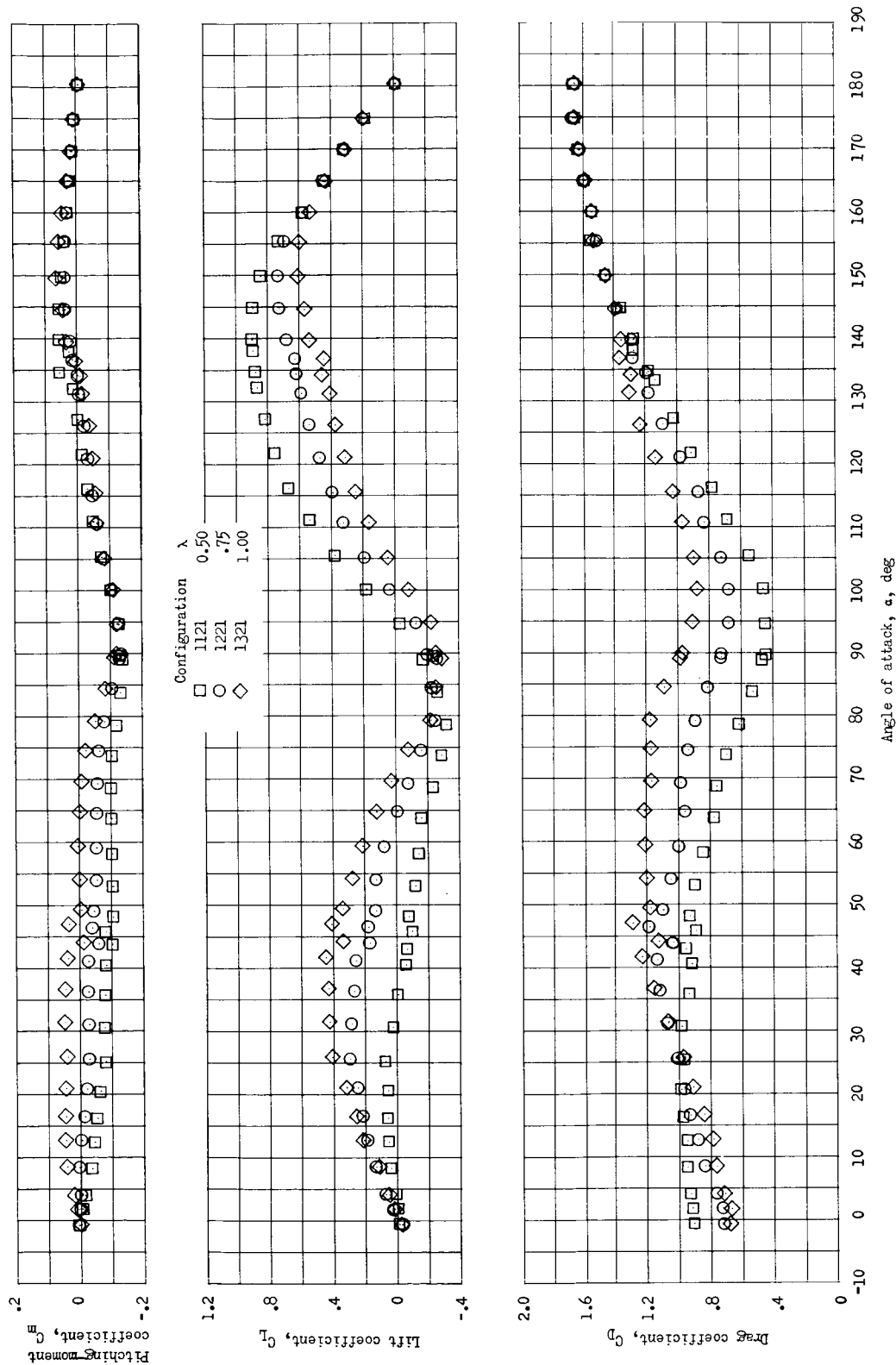
(a) Variation of C_m, C_L, and C_D with α.

Figure 8.- Effect of variations in fineness ratio on the longitudinal aerodynamic characteristics of a flat-base blunted cone with spherical nose and cone semiangle of 15°. Nominal M_∞ = 1.2.
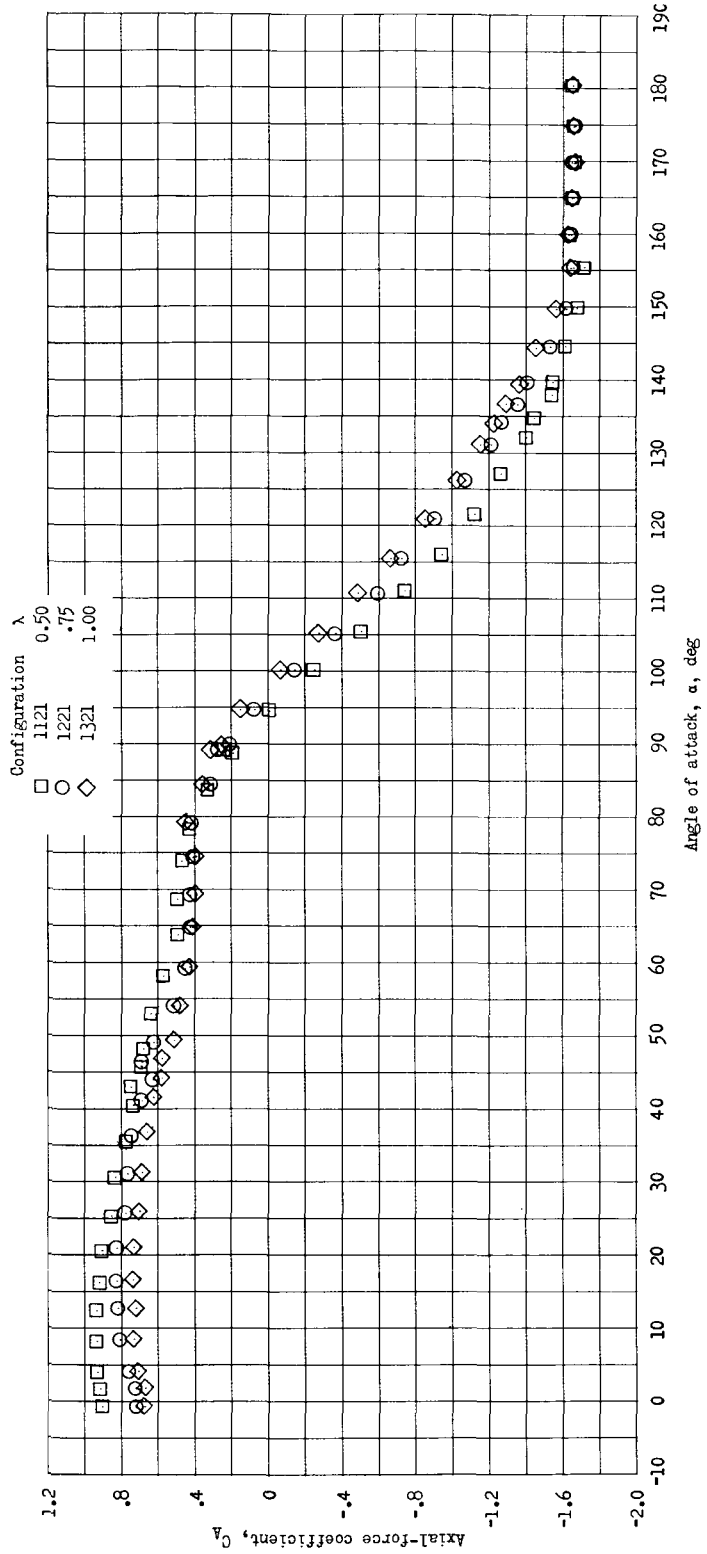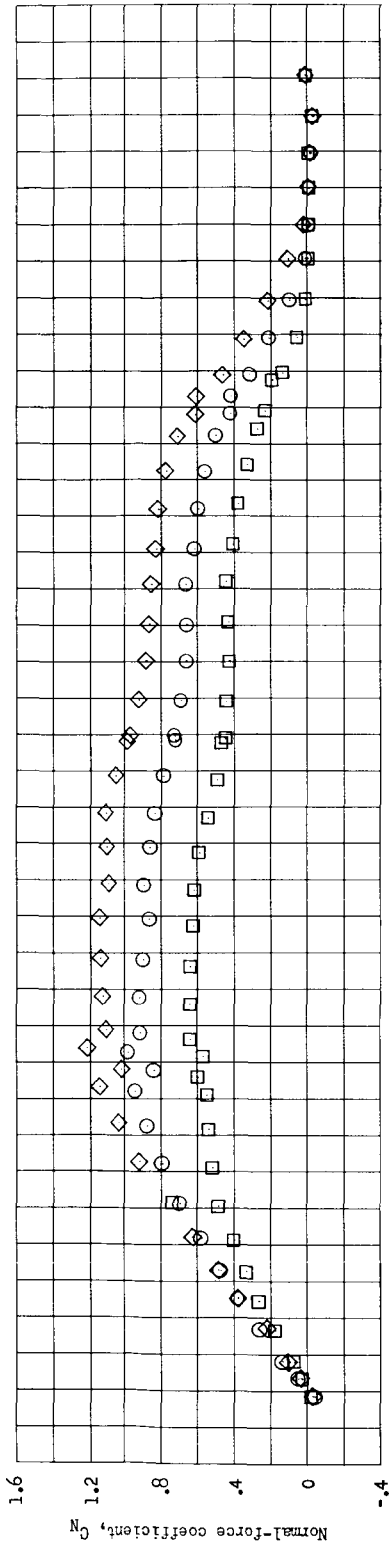
(b) Variation of C_N and C_A with α.

Figure 8.- Continued.

26
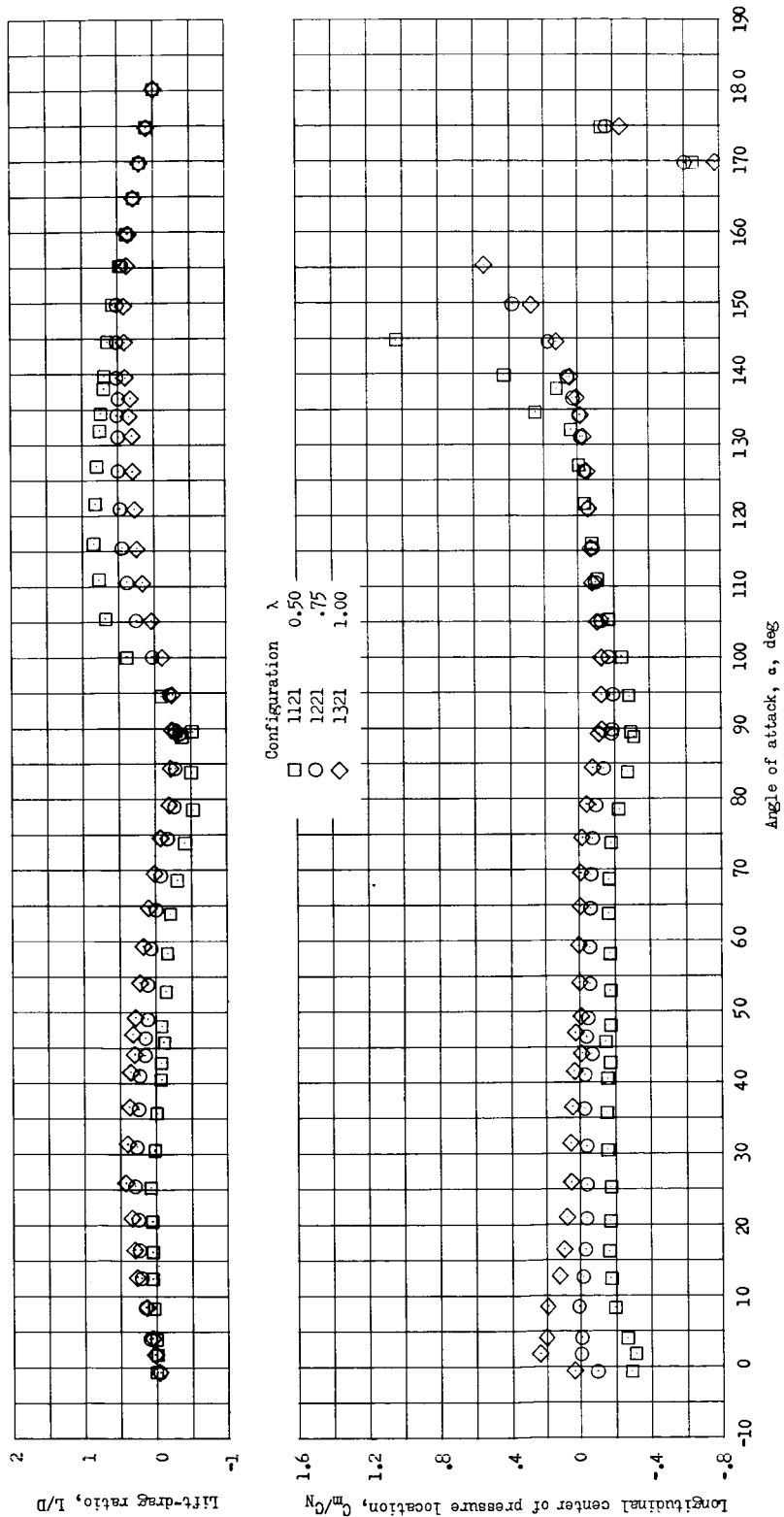
(c) Variation of L/D and C_m/C_N with α.

Figure 8.- Concluded.

Figure 9.- Effect of variations in cone semiangle on the longitudinal aerodynamic characteristics of a flat-base blunted cone with spherical nose and fineness ratio of 0.75. Nominal $M_\infty = 0.8$.
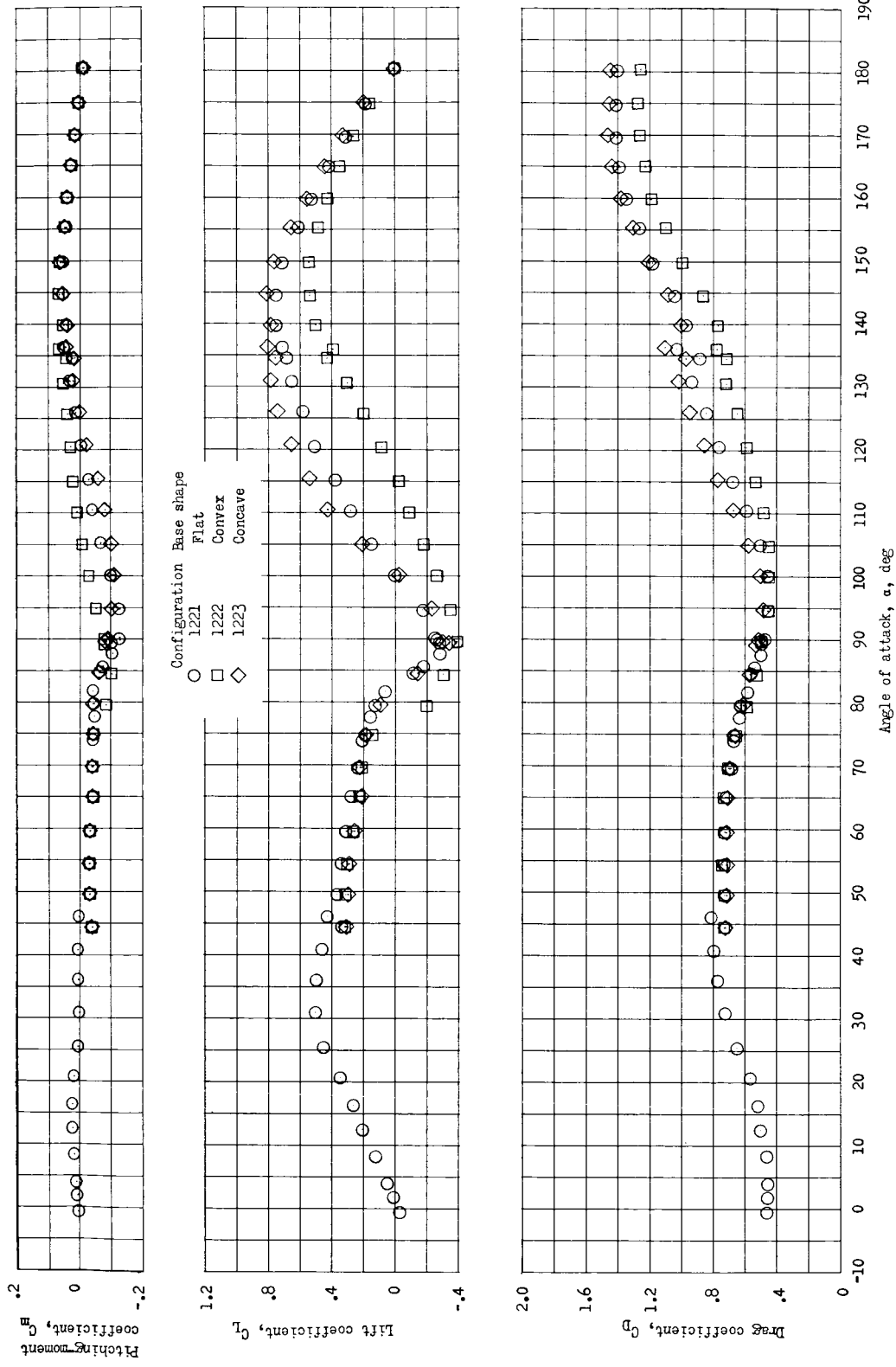
(a) Variation of C_m, C_L, and C_D with α.
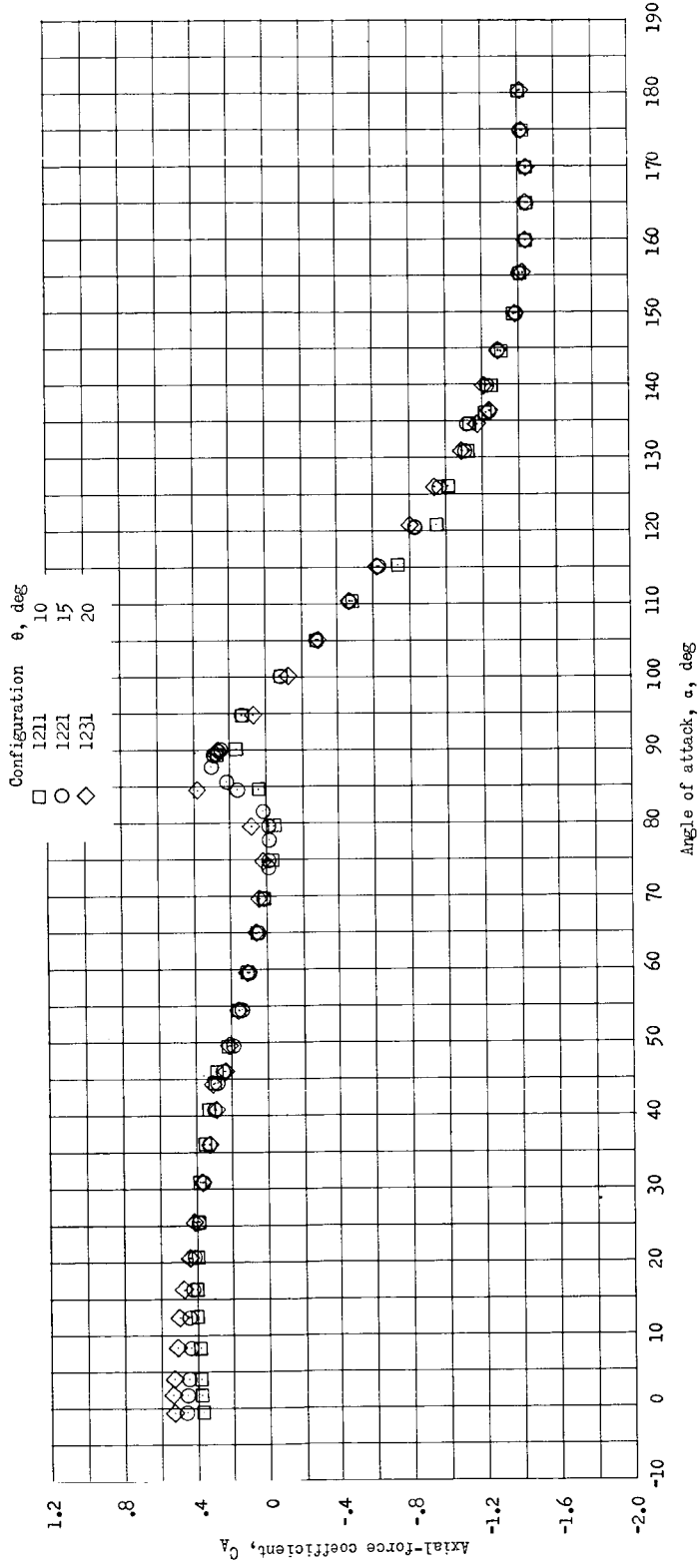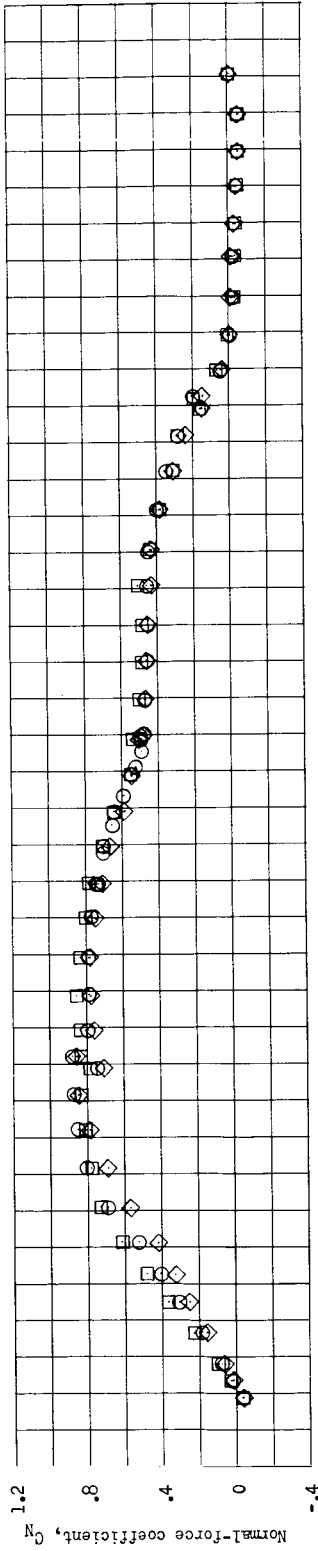
(b) Variation of C_N and C_A with α.

Figure 9.- Continued.

(c) Variation of L/D and C_m/C_N with α.

Figure 9.- Concluded.

(a) Variation of C_m, C_L, and C_D with α.

Figure 10.- Effect of variations in cone semiangle on the longitudinal aerodynamic characteristics of a flat-base blunted cone with spherical nose and fineness ratio of 0.75. Nominal $M_\infty = 1.2$.
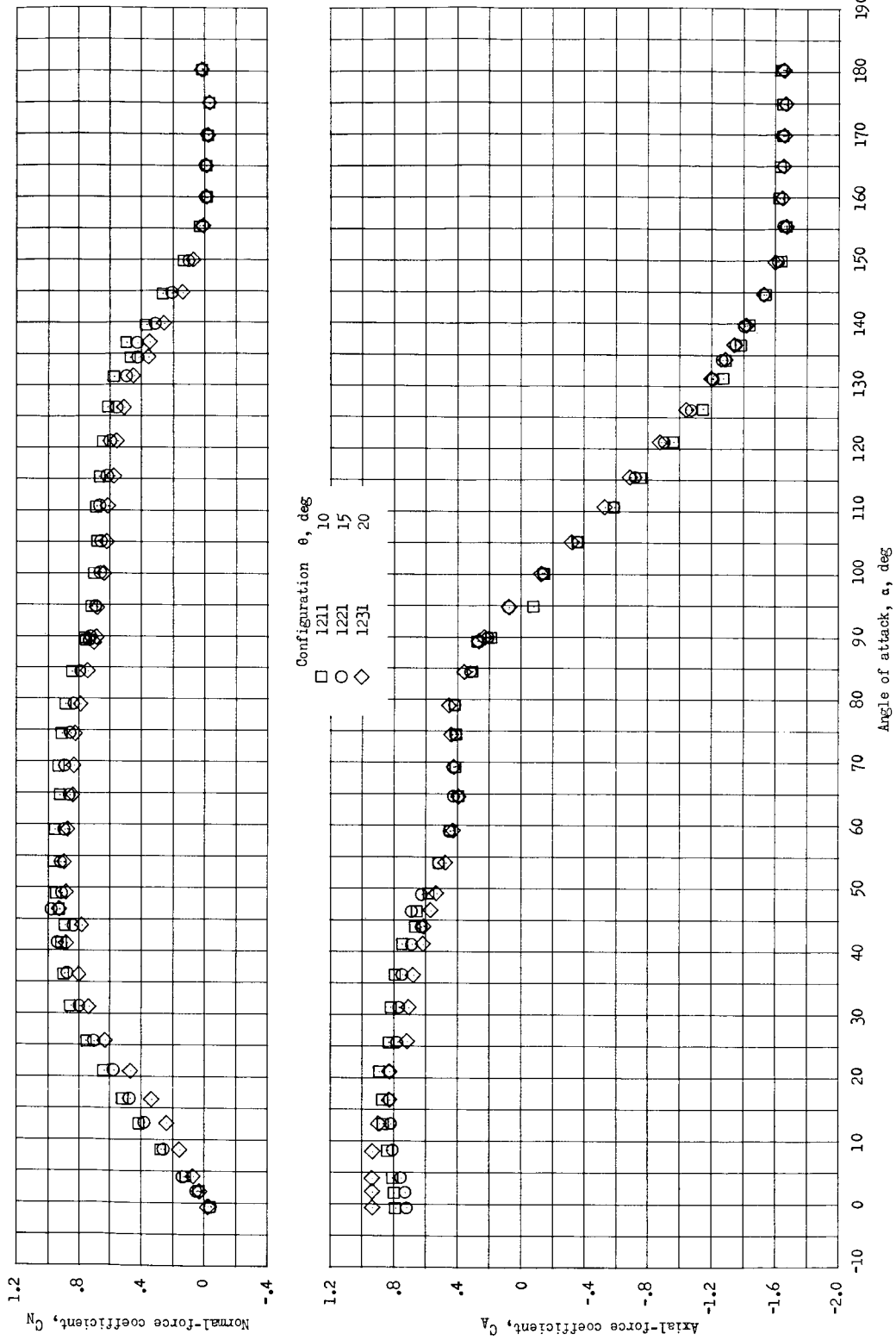
(b) Variation of C_N and C_A with α.

Figure 10.- Continued.
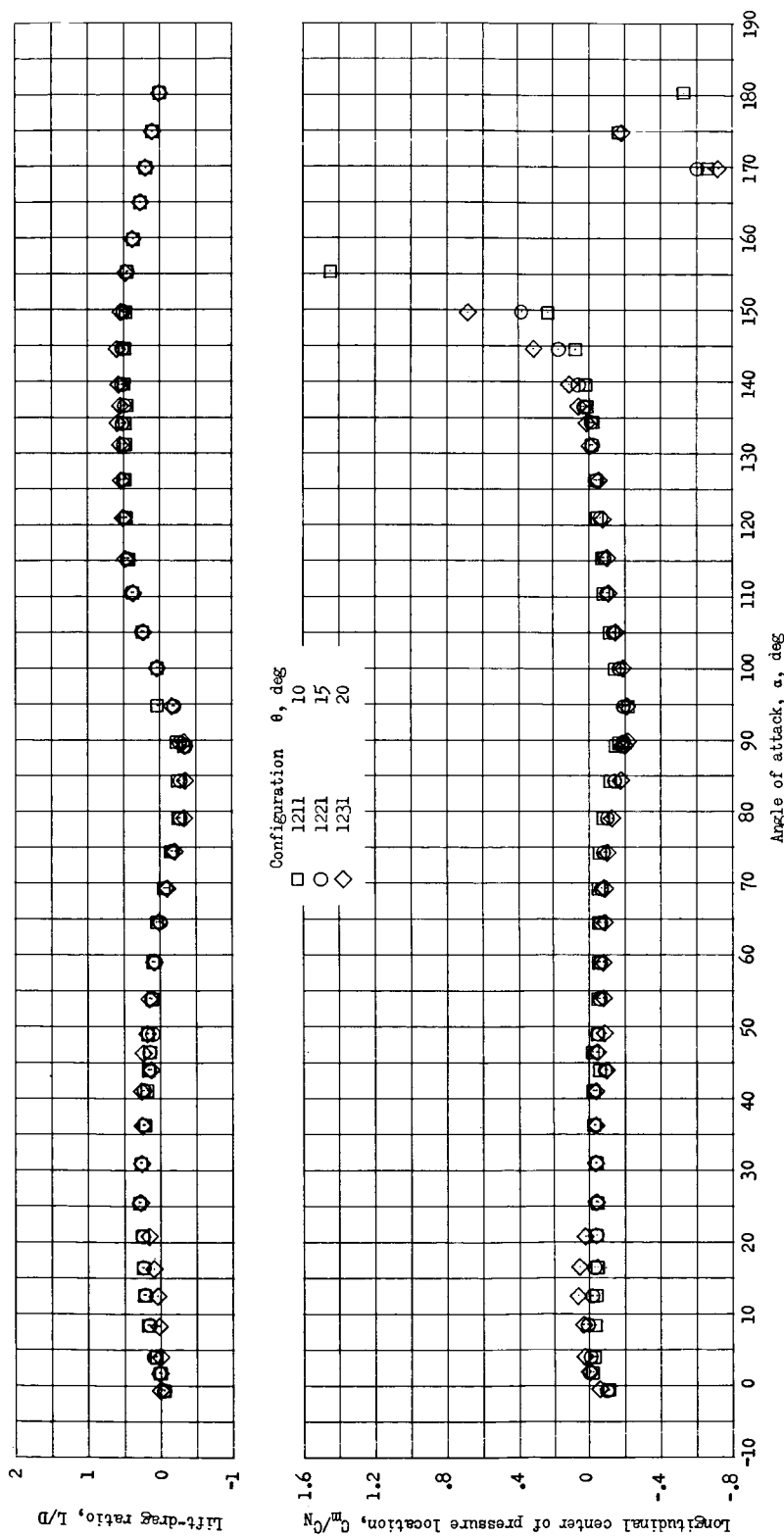
(c) Variation of L/D and C_m/C_N with α.

Figure 10.- Concluded.

(a) Variation of C_m, C_L, and C_D with α.

Figure 11.- Effect of variations in base shape on the longitudinal aerodynamic characteristics of a blunted cone with spherical nose, fineness ratio of 0.75, and cone semiangle of 15°. Nominal $M_\infty = 0.8$.
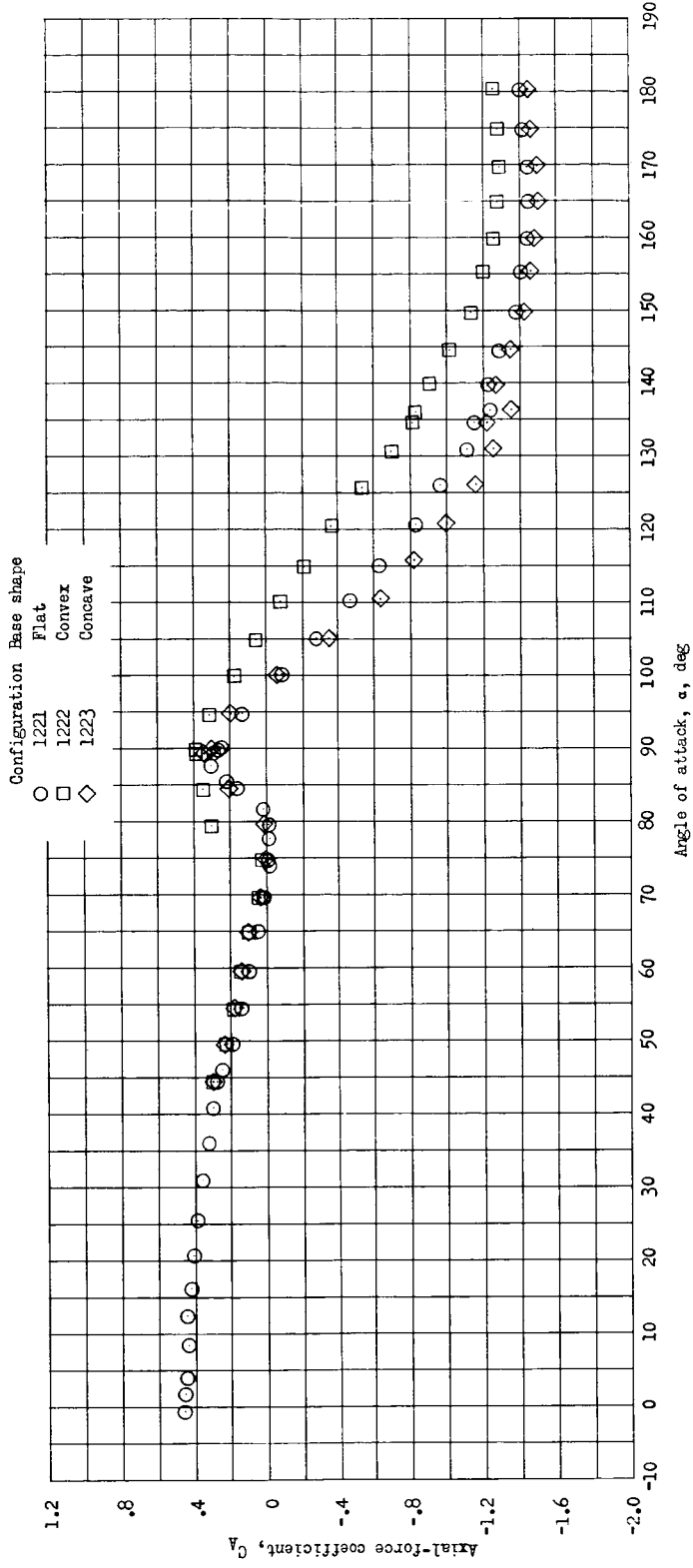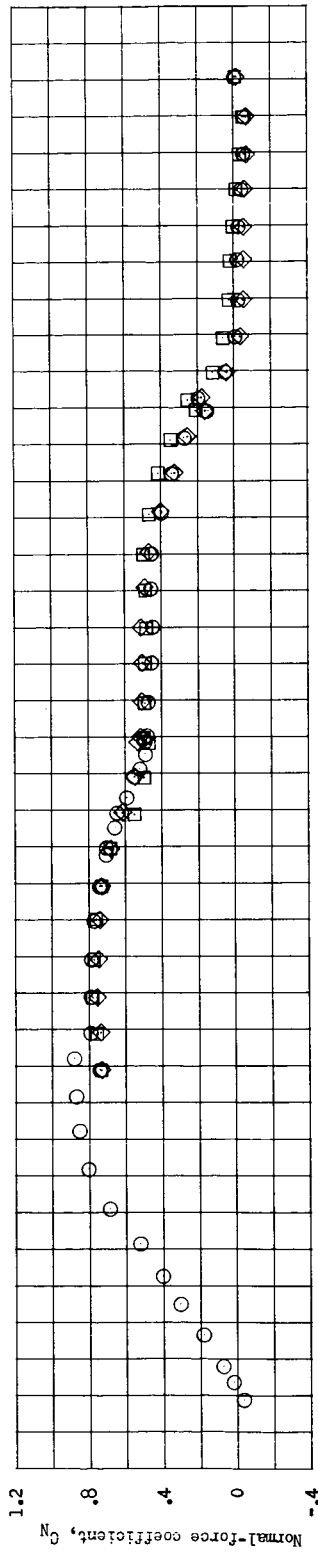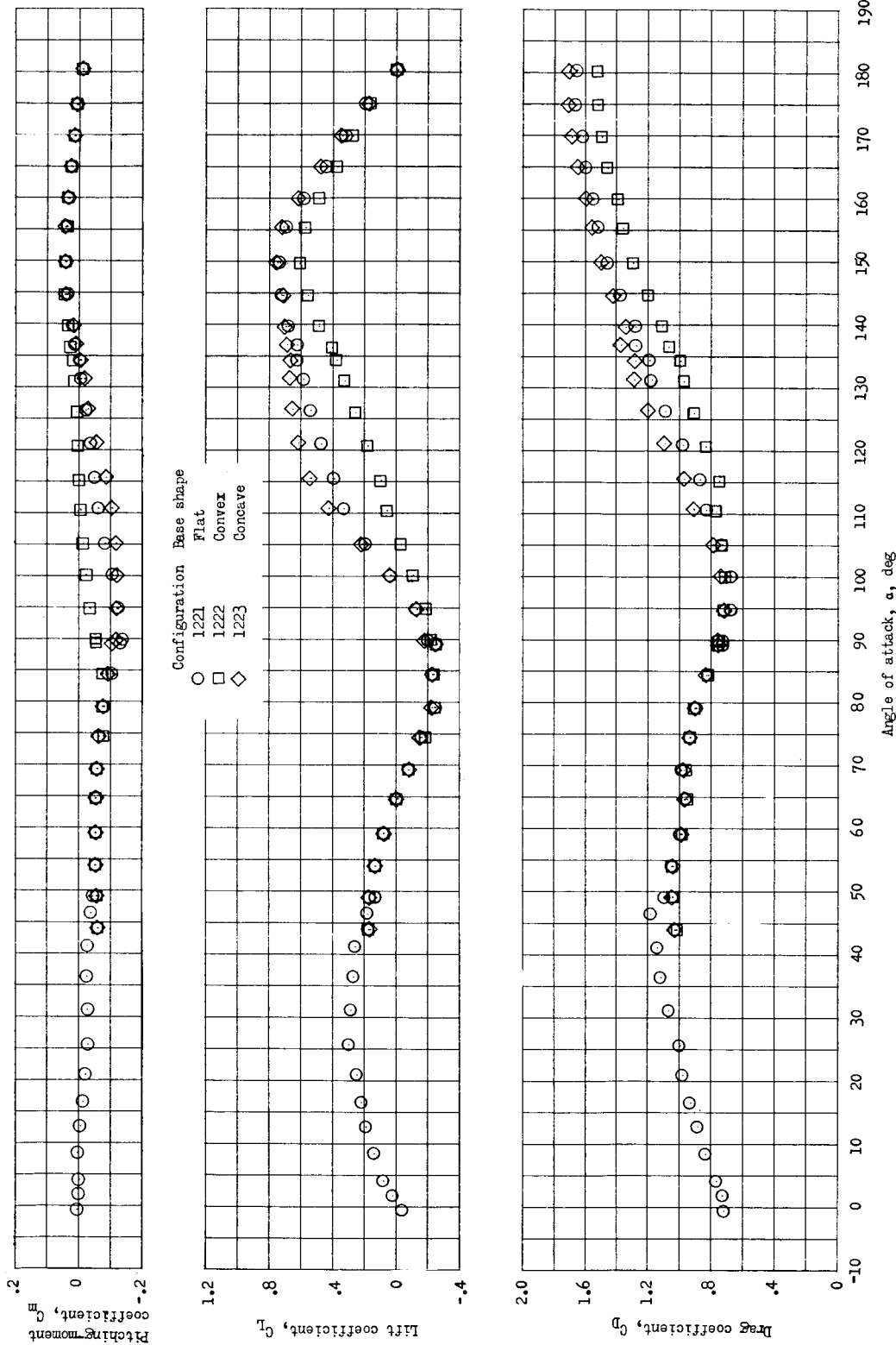
(b) Variation of C_N and C_A with α.

Figure 11.- Continued.
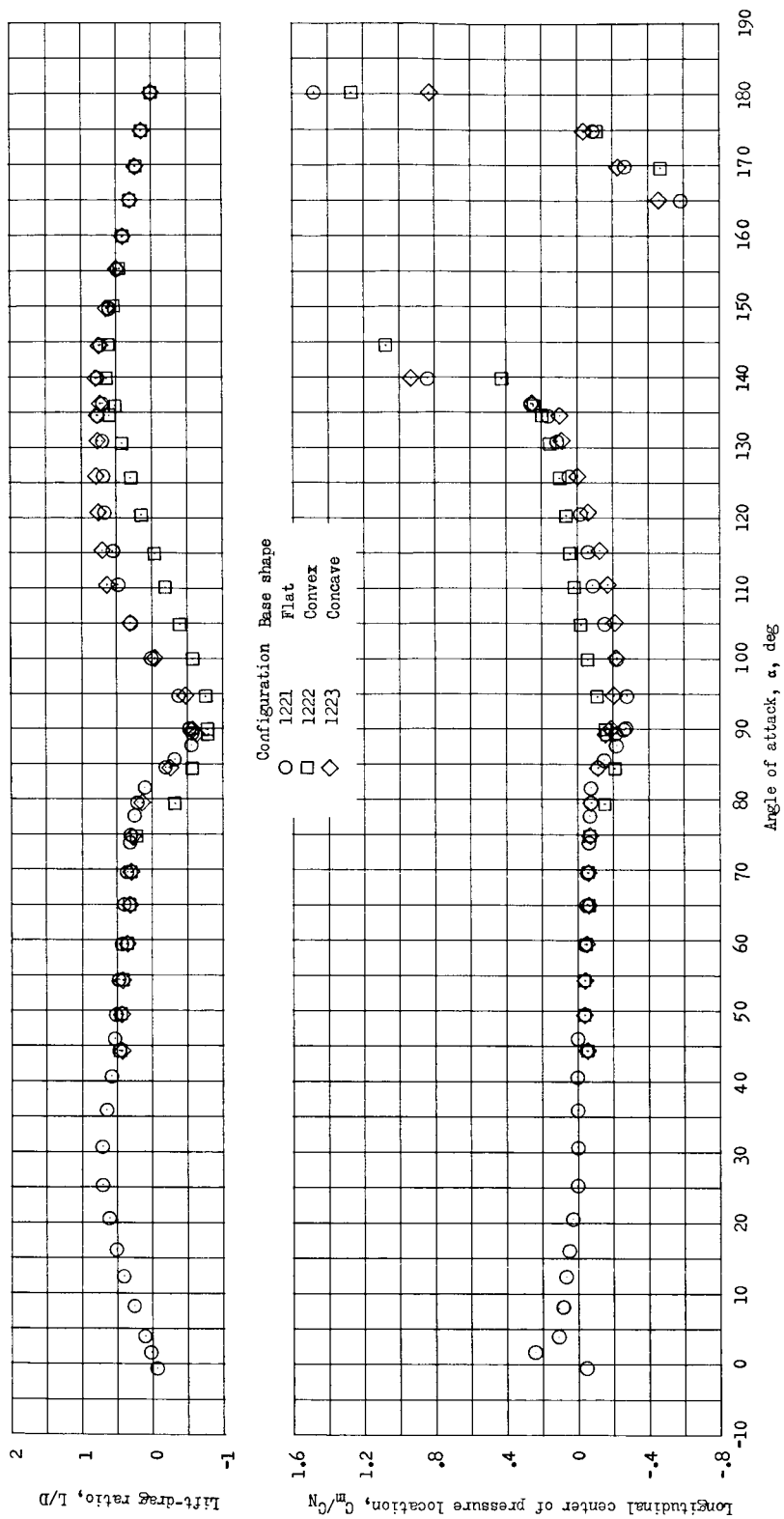
(c) Variation of L/D and C_m/C_N with α.

Figure 11.- Concluded.

(a) Variation of C_m, C_L, and C_D with α.

Figure 12.- Effect of variations in base shape on the longitudinal aerodynamic characteristics of a blunted cone with spherical nose, fineness ratio of 0.75, and cone semiangle of 15°. Nominal $M_\infty = 1.2$.
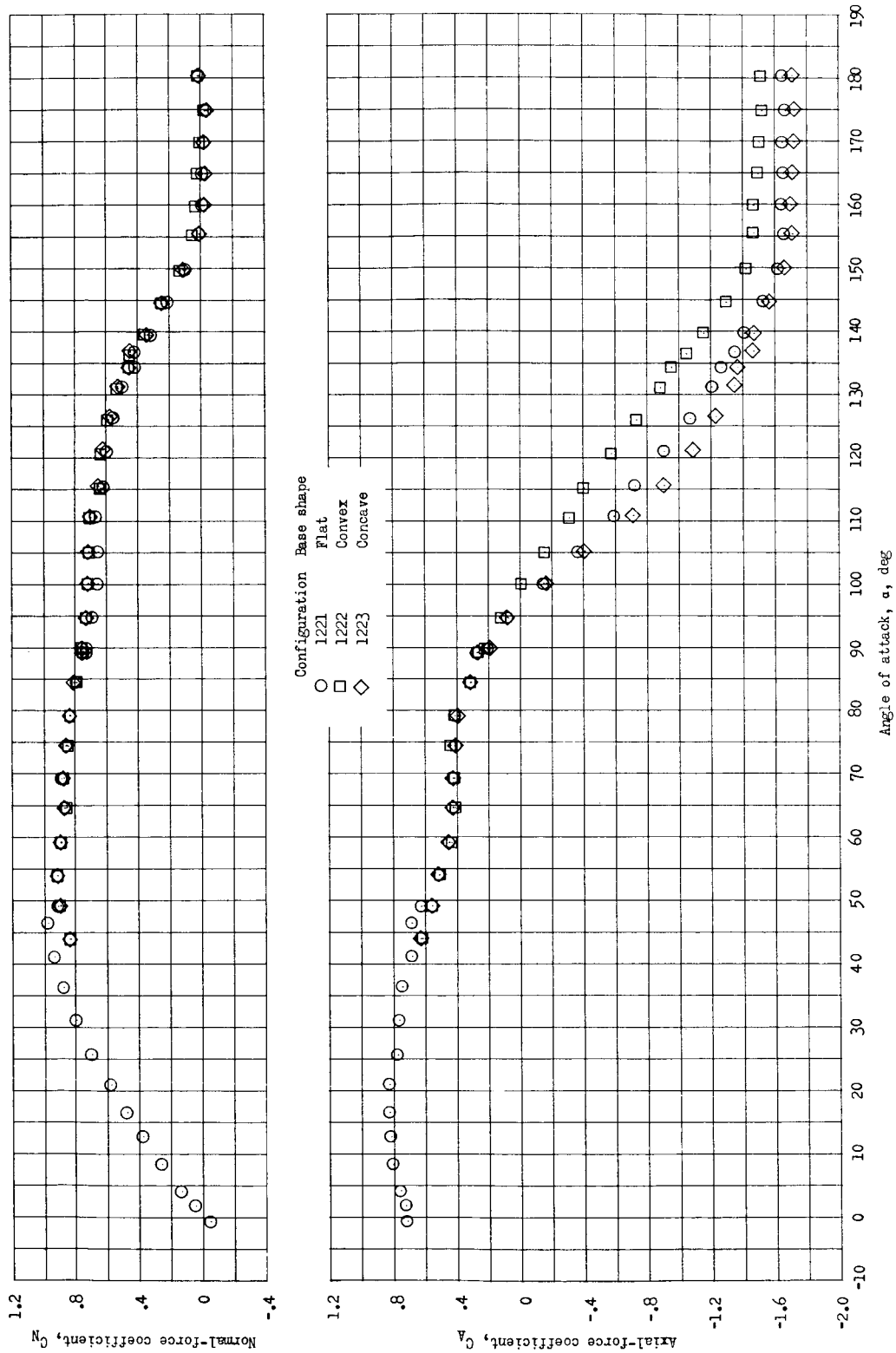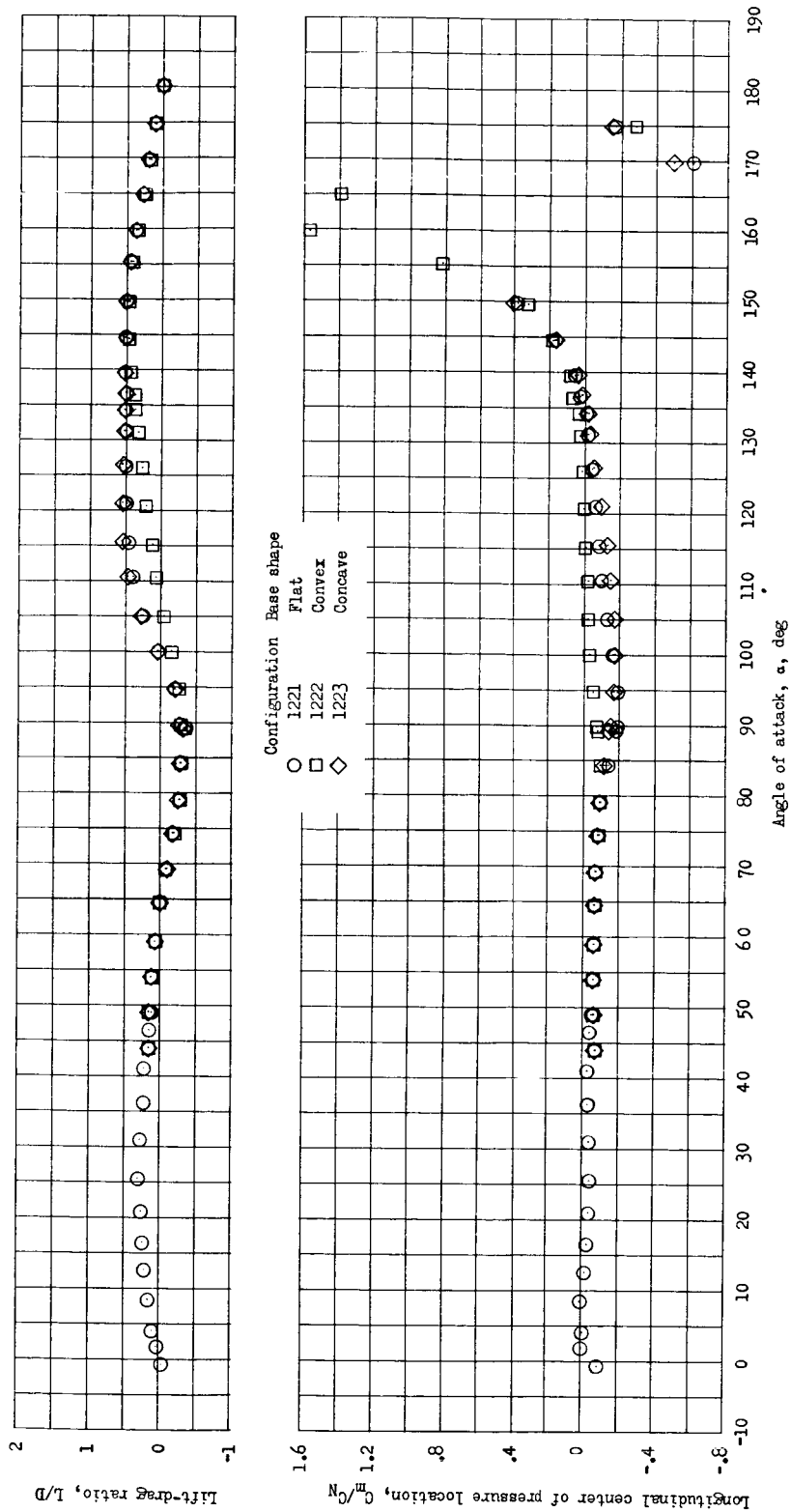
(b) Variation of C_N and C_A with α.

Figure 12.- Continued.

(c) Variation of L/D and C_m/C_N with α.
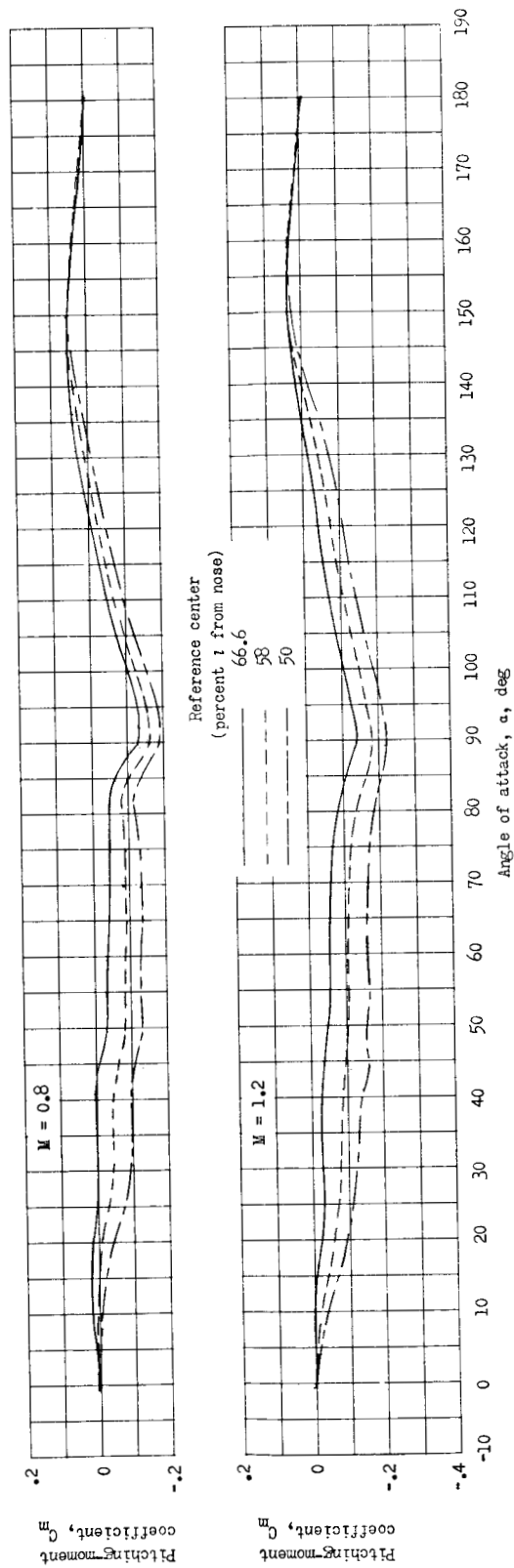
Figure 12.- Concluded.

Figure 13.- Effect of moment-reference-center location on the curve of C_m as a function of α of configuration 1221 at two Mach numbers.